SUMOylation of HSF1 orchestrates transcriptional and splicing programs during the proteotoxic stress response

Stefan MUELLER

ste.mueller@em.uni-frankfurt.de

Institute of Biochemistry II, Goethe University, Medical School, 60590 Frankfurt, Germany
https://orcid.org/0000-0002-8792-7700

Upayan Patra

Institute of Biochemistry II, Goethe University, Medical School, 60590 Frankfurt, Germany

Svenja Kuska

University of Göttingen, Department of General, Visceral and Pediatric Surgery

Thorsten Mosler

GU Frankfurt https://orcid.org/0000-0003-1800-2680

Timur Makarov

Institute of Molecular Biosciences, Goethe University Frankfurt, Frankfurt am Main, Germany

Urbi Mukhopadhyay

Institute of Biochemistry II, Goethe University, Medical School, 60590 Frankfurt, Germany

Christian Münch

Goethe University Frankfurt https://orcid.org/0000-0003-3832-090X

Ulrich Keller

Charité Universitätsmedizin Berlin https://orcid.org/0000-0002-8485-1958

Michaela Müller-McNicoll

Goethe-Universität Frankfurt am Main https://orcid.org/0000-0002-7174-8310

Matthias Wirth

University Medical Center Göttingen https://orcid.org/0000-0002-8340-0872

Article

Keywords:

Posted Date: July 17th, 2026

DOI: https://doi.org/10.21203/rs.3.rs-10283915/v1

Additional Declarations: There is **NO** Competing Interest.

Abstract

Proteotoxic stress poses a significant threat to cellular homeostasis. To maintain proteostasis, cells activate a multi-layered adaptive program that rewires translation, transcription, and splicing. However, the signaling events that coordinate this program are incompletely understood. Here we inhibited the ubiquitin-like SUMO pathway, subjected cells to transient heat stress, and performed integrative quantitative proteomic and transcriptomic analyses. Remarkably, in cells recovering from proteotoxic stress, inhibition of SUMO conjugation led to sustained activation of Heat Shock Factor 1 (HSF1). Mechanistically, loss of HSF1 SUMOylation promoted the persistent clustering of HSF1 at the promoters of its target genes and maintained its interaction with the general transcription machinery and transcriptional co-activators. This not only drives enhanced expression of canonical heat shock proteins, but also triggers persistent expression of long non-coding *HSATIII* RNAs that function as scaffolds for nuclear stress bodies (nSBs). Consequently, SUMO inhibition impaired the disassembly of nSBs and trapped splicing factors within these molecular condensates, thereby disrupting recovery of normal splicing patterns upon stress release.

Altogether, we define SUMOylation of HSF1 as a central regulatory node for restoration of proteostasis. Our data highlight the critical role of SUMO signaling in regulating the dynamics of a molecular condensate for ensuring timely resolution of the stress response and functional re-establishment of cellular homeostasis.

Introduction

Maintenance of genome and proteome integrity is essential for normal cellular function. To safeguard protein homeostasis, cells have evolved an elaborate and integrated proteostasis network. Proteotoxic stress represents a major threat to proteome integrity. Proteotoxic insults, such as heat shock or oxidative damage, induce protein misfolding, leading to their aggregation and ultimately contributing to the onset of proteinopathies such as neurodegenerative diseases [1,2]. As a countermeasure, cells activate protein quality control systems and deploy multilayered, tuneable stress-response pathways aimed at restoring proteostatic equilibrium [1,2]. To enhance the protein-folding capacity, cells upregulate the production of molecular chaperones. Concurrently, degradation pathways—the ubiquitin–proteasome system (UPS) and the autophagy–lysosome pathway—are activated to eliminate terminally misfolded proteins [2,3]. To further reduce the burden on these refolding and degradation systems under stress, cells transiently suppress splicing and translation, in part by sequestering components of the splicing and translation machineries together with mRNAs into stress-induced molecular condensates, such as the nuclear stress bodies (nSBs) and the cytosolic stress granules [4–6]

The heat shock response (HSR) represents a paradigmatic cellular survival program that is activated by proteotoxic stress. It is primarily orchestrated by the master transcription factor heat shock factor 1 (HSF1) [1]. Under non-stress conditions, HSF1 is maintained in an inactive monomeric state in the cytosol through interactions with molecular chaperones of the heat shock protein 70 (HSP70) and 90 (HSP90)

families. Upon stress, these chaperones are titrated away from HSF1 to bind accumulating misfolded proteins, enabling HSF1 trimerization and nuclear translocation. Trimeric HSF1 binds to cognate heat shock response elements (HSREs) in the promoters of heat shock genes, including those encoding molecular chaperones [7–10]. Subsequent HSF1-dependent transcriptional activation involves HSF1 phosphorylation and interactions with transcriptional co-regulators and chromatin-remodelling factors, which assemble into phase-separated transcriptional condensates [11–13]. In addition to canonical HSPs, HSF1 induces transcription of the *HSATIII* long non-coding RNA (lncRNA), which defines a distinct nuclear condensate known as nuclear stress bodies (nSBs). These structures sequester transcription and splicing factors, contributing to transcriptional attenuation and an altered splicing landscape [5,6,14,15]. Importantly, resolution of the HSR and recovery from stress rely on a negative feedback loop in which molecular chaperones inhibit HSF1 DNA binding and transactivation, thereby reverting HSF1 in its inactive state. The negative chaperone-mediated feedback does inhibit HSF1 activity only at the very terminal phase of the HSR, suggesting that other, understudied mechanisms for suppressing HSF1 activity contribute to the attenuation of the stress response.

Post-translational modifications, including ubiquitylation and SUMOylation, are integral components of the proteotoxic stress response. Both ubiquitylation and SUMOylation exhibit a global increase during acute stress, followed by a gradual decline upon stress resolution [16–18 19]. Attachment of ubiquitin or SUMO (SUMO-1 or the closely related SUMO-2/SUMO-3) to target proteins proceeds by a three-step enzymatic cascade involving dedicated conjugation and deconjugation machineries [20,21]. The modification occurs generally on lysine residues of target proteins and —besides mono-modification— can generate ubiquitin or SUMO chains of various linkage types as well as mixed SUMO-ubiquitin chains. Stress-induced ubiquitylation typically marks misfolded proteins for proteasomal degradation by the canonical UPS pathway [22], but non-proteolytic roles of ubiquitylation also contribute to stress resilience and recovery [23]. There is emerging evidence that SUMO signalling is instrumental for the re-establishment of protein homeostasis as a part of the proteotoxic stress response program [24,25]. We and others have demonstrated that a subset of misfolded, aggregation-prone proteins is cleared through SUMO-targeted ubiquitylation [26,27]. In this pathway, stress-induced SUMOylation primes substrates for subsequent ubiquitylation by SUMO-targeted ubiquitin ligases such as RNF4, RNF111, or TOPORS [28,29]. Moreover, in conjunction with ubiquitylation, SUMOylation is required for the proper disassembly of cytosolic stress granules (SGs) during recovery from proteotoxic stress [27], further supporting a role for SUMOylation in restoring cellular homeostasis upon stress resolution.

Despite these insights, a comprehensive and unbiased system-wide analysis of SUMO signalling in the proteotoxic stress response has been lacking. To address this gap, we pharmacologically inhibited SUMOylation by all three SUMO paralogs using the highly specific SUMO E1 inhibitor TAK-981, subjected cells to transient heat stress, and performed integrative quantitative proteomic and transcriptomic analyses. We found that during recovery from proteotoxic stress, SUMO inhibition maintains HSF1 in a persistent, transcriptionally competent state, resulting in sustained expression of canonical HSPs as well as the *HSATIII* lncRNA, leading to the formation of enlarged and persistent nSBs. We validated HSF1 as a

pivotal SUMO target orchestrating these effects. Consistently, expression of a SUMO-deficient HSF1 variant fosters formation of HSF1-induced nSBs, correlating with distinct alterations in the stress-regulated splicing landscape under SUMOi-primed condition. These findings identify SUMOylation of HSF1 as a central regulatory rheostat that enables timely attenuation of the heat shock response and cellular homeostasis.

Results

SUMO signalling reshapes the stress-regulated cellular proteome

To investigate the impact of SUMO signalling on the cellular proteome under acute proteotoxic stress and during the subsequent recovery phase, quantitative TMT-based proteomics was performed (Fig. 1A, C). Proteotoxic stress was induced by exposing HeLa cells to heat shock (HS) at 43°C for 1 hour, followed by a recovery phase of 2 hours at 37°C. To inhibit SUMO signalling under these conditions, cells were pre-treated with the highly specific SUMO E1 inhibitor TAK-981 (SUMOi) for 60 minutes prior to stress exposure (Fig. 1A, C, S1A). To detect alterations in the proteome that were due to ubiquitin-proteasome-mediated degradation in response to heat stress, proteasome inhibition was included as a separate condition when cells were recovering from stress (Fig. 1C). Consistent with published data, a subset of proteins (designated as cluster 1) exhibited reduced steady-state levels under acute heat stress (Figure S1B, C) and upon recovery from stress (cluster 1, 2) (Figure S1B, C, Table S1, S2) [23,30]. Proteasome inhibition largely prevented the depletion of these heat-sensitive proteins (cluster 1), validating the central role of the UPS in the clearance of misfolded proteins (Figure S1D, Table S2). Pre-treatment of cells with SUMOi had a more limited and selective effect on proteins that were downregulated during the heat stress response (Figure S1B), as exemplified by the stabilization of the SUMO ligase PIAS4 by SUMOi both under acute stress and in the recovery phase (Fig. 1B, D, Table S1, S2). PIAS4 is a well-established ubiquitylation substrate of the SUMO-targeted ubiquitin ligase RNF4, explaining its enhanced stability upon impairment of this pathway by SUMOi [31].

As part of the stress response, a specific subset of proteins was upregulated during acute heat stress (cluster 2) (Figure S1B) and upon recovery (cluster 3, 4) (Figure S1D, Table S2). GO term analysis of proteins whose expression is upregulated in the recovery phase reveals a strong enrichment of pathways connected to the cellular heat shock response (Figure S1F). Upregulated proteins include heat shock-inducible chaperones (HSPA1B, HSPA6, HSPH1, DNAJB1, DNAJB9, DNAJB4, BAG3) and stress-activated transcription factors (IER2, IER3, IER5, TFE3, ATF3, JUN, FOSL1, FOSB, HES1, BACH1, LRIF1, BHLHE40, ERRFI1, ELF3, ETS1, KLF3, PPARG) (Figure S1C, E, Table S2). Importantly, the MS data revealed that SUMO inhibition strongly enhances the steady-state levels of HSPA6 under acute stress and in the recovery phase (Fig. 1B, D). HSPA6 represents one of the most robustly induced HSP70 family members and anti-HSPA6 immunoblot analysis confirmed that SUMOi pretreatment strongly amplified the expression of HSPA6 in the post-HS recovery phase (Fig. 1E). Dose response and time course

experiments demonstrate that exposure of cells to SUMOi at a low concentration (0.2 μM) and for a short pre-treatment phase (30 min prior to HS) is sufficient to maintain persistent expression of HSPA6 for up to 8 hrs (Fig. 1E, S1G-I).

A hallmark of proteotoxic stress is the redistribution of misfolded proteins from the detergent-soluble to the detergent-insoluble cellular fraction [30,32]. We therefore asked whether under SUMOi treatment molecular chaperones become more engaged in the detergent-insoluble fraction. To this end, we performed quantitative MS of the NP-40 soluble and insoluble proteome in SUMOylation proficient and deficient cells (Fig. 1C). As predicted, a significant fraction of the proteins accumulated in the NP-40–insoluble fractions during acute heat stress (Figure S1J, Table S3, S4). Under SUMOi treatment, the covalent trapped SUMO-inhibitor adducts that are generated in the presence of TAK-981, were shifted to the soluble fraction under stress, validating the on-target activity of the inhibitor (Fig. 1F). Importantly, however, SUMOi treatment led to the enrichment of HSPA6 as well as other HSP70 chaperones and HSP40 co-chaperones in the insoluble fraction during the HS recovery phase (Fig. 1F, S1K, Table S4). Immunoblotting of selected HSP family members validated these findings (Fig. 1G). Altogether, these data suggest that inhibition of SUMOylation exacerbates the cellular response to heat stress.

Importantly, this effect was not restricted to heat stress but was also observed in response to a broad spectrum of proteotoxic insults, including proteasome inhibition or treatment with sodium arsenite or cadmium chloride (Figure S1L- N). Furthermore, the induction of HSPA6 by gamitrinib–triphenylphosphonium (GTPP), a mitochondrial HSP90 inhibitor that induces mitochondrial protein misfolding, was more pronounced in SUMOylation-deficient cells (Figure S1O). Proteomic analysis of the insoluble fraction from GTPP-treated cells revealed an increase of multiple stress-induced chaperones and co-chaperones – including DNAJB1, HSPH1, CREB3L2, AHSA1, HSP90AA1, HSP90AB1, HSP90B1, DNAJC7, and DNAJC9 – upon inhibition of SUMOylation (Figure S1P, Table S5). Collectively, these data indicate that SUMOylation broadly constrains the proteotoxic stress response across diverse stress modalities.

SUMOylation attenuates HSF1-driven gene expression programs

The induction of HSPs in response to proteotoxic stress represents a coordinated adaptive gene expression program orchestrated by HSF1 [7–10]. Gene ontology term (GO_Biological Process) and Curated Reactome analyses of proteins upregulated upon SUMOi treatment in cells recovering from heat stress revealed a strong enrichment of pathways connected to protein folding and HSF1-dependent transactivation indicating that the heat shock response is amplified under conditions of impaired SUMO conjugation (Figure S2A, B). To assess whether SUMO signalling modulates stress response programs at the RNA level in an HSF-1-dependent manner, we performed unbiased RNA-seq analyses in HSF1 proficient (HSF1 WT) and deficient (HSF1 KO) HeLa cells [33] subjected to acute heat stress and recovery in the presence or absence of SUMO inhibition (Fig. 2A, S2C). Fully consistent with the proteome rewiring described above, GO term enrichment and Curated Reactome analysis of mRNA alterations again

revealed protein folding and HSF1 activation as the most highly enriched upregulated pathways under SUMOi in the acute stress phase and the recovery phase, respectively (Figure S2D). Unbiased clustering of the differentially expressed genes sorted by SUMOi-depedendent regulation revealed 8 distinct clusters (Figure S2E). GO term (GO_Biological Process) analyses of cluster 8 confirms activation of the cellular heat shock response during the HS recovery phase and further enrichment of this cluster in the absence of SUMOylation (Figure S2E, F). Agreeably, gene set enrichment analysis (GSEA) demonstrated that SUMO inhibition exerted the most pronounced effects on the Curated Reactome pathways associated with HSF1-dependent transactivation, both during acute stress and in the recovery phase (Fig. 2B). Under SUMOi-treated conditions, running-sum enrichment scores demonstrated a strong overrepresentation of HSF1 target genes at the top of the ranked gene lists during both heat stress and recovery, indicating that a greater number of HSF1 target genes are among the most highly upregulated transcripts and that their expression levels are further elevated when SUMO conjugation is impaired (Fig. 2B). We identified a number of transcripts for HSP70/HSP40 chaperones, including *HSPA6*, showing elevated HS-induced expression upon inhibition of SUMOylation (Fig. 2C). Importantly, HSF1 KO cells failed to generate this enrichment signature (Fig. 2D). In fact, GSEA revealed depletion of “Regulation of HSF1-mediated heat shock response” in SUMOi-primed HSF1 KO HeLa cells during the recovery phase (Fig. 2D). Taking *HSPA6* as a prevalent HSF1-driven candidate gene, we further validated by qRT-PCR that SUMOi can boost the induction of *HSPA6* mRNA both during HS and post-HS recovery phase (Fig. 2E). Consistently, targeted inhibition of HSF1-dependent transcription by a small molecule KRIBB11 [34] abolished HS-driven HSPA6 expression even under SUMOi-primed conditions (Figure S2G). Together, these results demonstrate that SUMOi treatment leads to stronger and more sustained activation of HSF1-dependent gene expression, characterized by increased transcriptional output of canonical heat shock genes and prolonged HSF1 activity during both acute stress and recovery.

The induction of proteotoxic stress by proteasome inhibitors, such as bortezomib or carfilzomib, is a cornerstone of multiple myeloma therapy and we recently demonstrated that SUMOi exhibits synthetic lethality with proteasome inhibition in cellular models of multiple myeloma [35]. Re-evaluating the available transcriptomics data from two different multiple myeloma cell lines OPM2 and JJN3 [35] revealed that combinatorial targeting of the proteasome and SUMO pathway led to a highly synergistic activation of HSF1-driven proteotoxic stress response correlating with reduced viability (Fig. 2F, S2H). Therefore, these data suggest that SUMOylation exerts an inhibitory role on HSF1-driven gene expression, contributing to cell survival under high proteotoxic burden.

SUMO-2/3 conjugation to HSF1 controls the HSF1-driven proteotoxic stress response

The data described above indicate that SUMO signalling attenuates HSF1-driven gene expression. To determine whether this effect is mediated by conjugation of SUMO-1 or SUMO-2/3 paralogs, we selectively depleted either SUMO-1 or SUMO-2/3 by siRNA before heat stress (Fig. 3A). Notably, very much like SUMOi treatment, depletion of SUMO-2/3, but not SUMO-1, led to enhanced HSPA6 expression

during the post-HS recovery phase (Fig. 3A). Further, while SUMO-1 silencing did not affect SUMOi-induced HSPA6 expression, depletion of SUMO-2/3 completely abolished this response, demonstrating that SUMO-2/3–mediated signalling determines HSF1-dependent gene expression under heat stress (Fig. 3A). SUMO-2/3-depleted cells also displayed an enhanced HSPA6 response upon induction of proteotoxic stress by the proteasome inhibitor MG-132, indicating that SUMO-2/3 controls HSPA6 expression in response to different types of proteotoxic stress (Figure S3A).

We next addressed whether the alteration in HSF1-driven gene expression caused by SUMOi are a direct consequence of impaired HSF1 SUMOylation. HSF1 has been reported to undergo SUMOylation following heat stress, but reports on the functional consequences of this modification are conflicting [36–38]. Ni-NTA pulldown experiments confirmed SUMO-2 conjugation to endogenous or Flag-tagged exogenous HSF1 (Figure S3B, C). Previous work mapped K298 as a major SUMO attachment site in HSF1, but our own and published high-throughput analyses identified at least six lysine residues in HSF1 as potential SUMO acceptor sites [36,37,39–41] (Fig. 3B). To identify the relevant heat-induced site(s), we generated a series of lysine-to-arginine mutants and assessed the SUMOylation status of Flag-tagged HSF1 variants following co-expression of His-tagged SUMO-2 and Ni-NTA enrichment (Fig. 3C, S3D). Wild-type HSF1 showed robust SUMOylation under basal condition and upon exposure of cells to heat stress (Fig. 3C). By contrast, the HSF1^{K298R} mutant as well as all HSF1 variants harbouring the K298R mutation were completely devoid of SUMOylation (Fig. 3C, S3D), validating K298 as the major SUMO acceptor site. Because K298 resides within a canonical KxE SUMOylation motif, we next examined whether mutation of the flanking + 1 and + 2 acidic residues E299 and E300 affects SUMO conjugation. Similar to the K298R mutant, either single or combined alanine substitution of E299 and E300 abolished SUMOylation of HSF1 both under basal conditions and upon heat stress (Fig. 3D).

We next investigated whether SUMO-deficient HSF1 affects the expression of the model target HSPA6. To this end, we established an inducible knockdown-complementation system in which siHSF1-resistant Flag-HSF1^{WT} or Flag-HSF1^{K298R} was integrated in the HeLa genome as a single-copy transgene by targeted recombination under the control of a doxycycline-inducible promoter. In this cellular background, upon siRNA-mediated depletion of endogenous HSF1 and re-expression of wild-type HSF1, HSPA6 expression was induced during the recovery phase following heat stress (Fig. 3E, S3E, S3F). Moreover, SUMOi treatment further enhanced HSPA6 expression, validating the experimental system (Fig. 3E). Strikingly, under the same conditions, re-expression of the SUMO-deficient Flag-HSF1^{K298R} variant resulted in elevated HSPA6 steady-state levels that were not further increased by SUMOi treatment (Fig. 3E). The same was found to be true for proteotoxic stress induced by proteasome inhibition (Figure S3G). By following the kinetics of HSPA6 expression in the post-HS recovery phase, Flag-HSF1^{K298R} drove elevated and persistent expression of HSPA6 up to 6 hours after HS, while HSPA6 expression was largely dampened in cells expressing wild-type Flag-HSF1 (Fig. 3F). These data indicate that SUMOylation of HSF1 itself functions as a brake on HSF1-mediated transactivation. Importantly, expression of the SUMO-deficient HSF1$^{E299/300A}$ mutant phenocopied the effects of the HSF1^{K298R} variant on HSPA6 expression (Fig. 3G), ruling out the possibility that loss of other post-translational

modifications at K298 causes enhanced HSPA6 expression. Altogether, our data suggest that SUMO-2 conjugation to K298 attenuates the magnitude and duration of the HSF1 transcriptional program.

SUMOylation controls the association of HSF1 with transcriptional co-regulators

To get insight into how SUMO signalling rewires HSF1-driven transcriptional programs, we expressed UltraID-tagged HSF1 and performed proximity proteomics under non-HS and HS conditions in presence and absence of SUMOi (Fig. 4A). Functional enrichment analysis based on the Curated Reactome annotations shows the enrichment of RNA processing and splicing factors as well as components of the DNA repair, transcription machineries, and epigenetic regulators in the HSF1 proximity proteome and this enrichment signature is also pronounced under heat stress, recapitulating the published data [42,43] (Fig. 4B, S4A, Table S6). Importantly, however, the comparison of the HSF1 proximity-proteomes in SUMO proficient and deficient cells revealed that SUMOi treatment favoured the interaction of HSF1 with the general transcription machinery (TFIIB, TFIIF and TFIIE) as well as components of histone-acetyl transferase (HAT)-containing transcriptional co-activator complexes (TADA3, CRTC2) and SWI/SNF chromatin remodelling complexes (SMARCD3) (Fig. 4C). The enhanced engagement of transcriptional co-activators and the basal transcription machinery in SUMOi-treated cells suggest that in SUMO-deficient cells HSF1 is in a more active transactivation-competent state. To validate the importance of HAT and SWI/SNF for HSF1-mediated expression of our model target HSPA6 under stress, we used small-molecule p300/CBP inhibitor A-485, CREB/CRTC2 interaction inhibitor A57, and SMARCA2/4 targeting PROTAC AU-15330 (which functionally inactivates the SWI/SNF complex). Interestingly, all these small molecules sensitized stress-activated HSPA6 expression even in the presence or absence of SUMOi (Fig. 4D, E; S4B, C, D, E). When combining both A-485 and AU-15330, HS-driven HSPA6 expression was heavily reduced and could not be rescued by SUMOi treatment or expression of $HSF1^{K298R}$ (Fig. 4E, S4F). Altogether, these data are consistent with the idea that the inhibition of SUMO signalling engages multiple co-activator complexes and allows a more productive RNA Pol II engagement on HSF1-controlled genes, thereby enabling rapid and high-amplitude transcription of stress-response genes. In line with this idea, CUT&RUN (Cleavage Under Targets and Release Using Nuclease) experiments demonstrate that SUMOi induces the preferential enrichment of HSF1 at canonical HSF1 binding elements and its persistent accumulation at the transcriptional start sites (TSS) of HSP70 and HSP40 family members without affecting global TSS binding of HSF1. Notably, in combination with SUMOi, HSF1 occupancy becomes more sharply focused on high-confidence HSF binding sites, with the top-ranking peaks corresponding almost exclusively to canonical HSF motifs, an effect not observed under heat shock alone, where binding is more broadly distributed across additional non-canonical sites. (Fig. 4F, G, Figure S4G, H, Table S7).

SUMO signalling affects the dynamics of nSBs and rewires RNA processing

Upon sensing proteotoxic stress, HSF1 promotes transcription of the non-coding *HSATIII* RNA by binding to heat shock elements within HSATIII DNA. *HSATIII* RNAs remain proximal to their transcription sites and serve as scaffolds for the assembly of nSBs. These molecular condensates sequester transcription and splicing factors, thereby reshaping the alternative splicing program [5,6,14]. CUT&RUN analysis of cells exposed to heat stress revealed enhanced binding of HSF1 to the *HSATIII* locus in the presence of SUMOi (Fig. 5A). Consistent with this observation, induction of *HSATIII* RNA during HS recovery phase was further fostered upon SUMOi treatment (Fig. 5B), strengthening the notion that SUMOylation attenuates HSF1-driven transcription. Given the role of *HSATIII* RNA as a scaffold for nSBs, we examined nSB dynamics upon SUMOi treatment using anti-HSF1 immunofluorescence. Heat stress typically induced the formation of HSF1-positive stress bodies inside the nucleus. Intriguingly, SUMOi treatment resulted in markedly enlarged nSBs under acute stress conditions (Fig. 5C, Figure S5A, B). Moreover, during the recovery phase, larger nSBs persisted in SUMOi-treated cells, demonstrating that SUMO signalling is required for proper resolution of the proteotoxic stress response (Fig. 5C, Figure S5A, B). The impact of SUMOi on nSB enlargement under HS was abrogated when general or HSF1-mediated transcription was blocked by the BRD4/BET degrader dBET6 or the HSF1 inhibitor KRIBB11, respectively, consolidating the hypothesis that SUMO signalling affects nSB dynamics by fostering active HSF1-dependent transcription (Figure S5C, D, E). Importantly, expression of Flag-HSF1^{K298R} phenocopied the effects of SUMOi treatment by inducing the formation of enlarged HSF1-positive nSBs, thus demonstrating that this effect is directly mediated by HSF1 SUMOylation (Fig. 5D, S5F). Collectively, these data suggest that SUMO-deficient HSF1 promotes *HSATIII* RNA expression, thereby fostering the formation and perturbing the resolution of nSBs.

nSBs serve as hubs for stress-induced sequestration of RNA-binding proteins and act as a "sponge" to repress pre-mRNA splicing during heat stress recovery [5,6,14]. To investigate whether nSBs assembled by wild-type or SUMO-deficient HSF1 differ and engage distinct protein interaction networks under heat stress, we performed proximity proteomics by expressing UltraID-tagged HSF1^{WT} or HSF1^{K298R} in HSF1 KO HeLa cells. After heat stress and proximity-dependent biotinylation, HSF1-associated proteins were captured on NeutrAvidin beads and analyzed by mass spectrometry (Fig. 5E). Both the HSF1^{WT} and HSF1^{K298R} interactomes revealed an enrichment of proteins involved in transcription and splicing including proteins previously identified as nSB constituents (Table S8) [14]. However, strikingly, a quantitative comparison revealed that the HSF1^{K298R} interactome is enriched with the highly interconnected network of splicing factors that normally reside in nuclear speckles, including SRSF6, LUC7L2, LUC7L3, TRA2B, SRRM1, SRRM2, SON, PRPF38B, PPIG and SNRNP70 (Fig. 5F, G, S5G). The larger size and the impaired resolution of nSBs during heat shock recovery suggest that the activity and availability of these splicing factors is affected.

To test whether the disturbance of nSB dynamics affects general splicing patterns, we analysed our RNASeq data for alterations in intron retention using an unbiased clustering approach (Figure S5H). We identified 8 clusters, with clusters 3, 5 and 8 showing the highest levels of intron retention during heat shock recovery. This is in line with the known role of nSBs in promoting retention of introns during the

recovery phase from heat shock [14]. However, only a smaller subset of those introns was affected by SUMOylation inhibition. We identified 401 introns that were more retained and 165 introns that were better spliced upon SUMOi treatment. Interestingly, the more retained introns were found in genes involved in histone modification and negative regulation of gene expression (Figure S5I), suggesting that SUMO-signaling controls a specific subset of introns. To test whether the regulated introns correspond to detained introns that were previously associated with nSBs and that are important for the stress response [14], we analyzed their features. Introns that were better spliced upon SUMOi treatment were much shorter in length, had weaker 3' splice sites and were significantly more conserved than non-affected genes (Fig. 5H, I, J), which are prominent features of detained introns [14,44]. However, they did not show longer flanking exons, weaker 5' splice sites or a higher GC content (Figure S5J, K), suggesting that they represent a distinct group. Similarly, the more retained introns showed higher GC content, shorter length and better conservation, but their splice sites were even stronger than non-regulated introns, indicating that they are spliced well under normal conditions (Fig. 5H, J, S5K). These data suggest that the observed changes in nSB dynamics and composition alter the splicing landscape during heat shock recovery. Altogether, these findings support a model in which SUMOylation is needed to attenuate and resolve HSF1-driven transactivation, thereby facilitating the clearance of nuclear stress bodies during the recovery phase. This coordinates the shutdown of canonical heat shock protein transcription with proper RNA processing.

Discussion

The transcription factor HSF1 orchestrates the cellular response to proteotoxic insults by initiating a multi-layered adaptive pathway [9,10,45]. The timely resolution of this response is instrumental for the restoration of proteostasis. Here, we identify SUMOylation of HSF1 as a regulatory rheostat that balances the magnitude and duration of HSF1-driven transcription by limiting its engagement with transcriptional co-regulators and attenuating the expression of molecular chaperones. Further, SUMOylation of HSF1 is essential for the proper resolution of nuclear nSBs and the re-establishment of the splicing landscape upon stress relief, defining SUMOylation of HSF1 as a tuneable molecular switch that enables cells to recover from stress.

Our study demonstrates that SUMOylation actively shapes the recovery phase of the proteotoxic stress response. Inhibition of SUMO conjugation, depletion of SUMO-2/3, or expression of SUMO-deficient HSF1 all resulted in stronger and more sustained induction of HSF1 target genes, including HSPA6, across multiple stress conditions. Thus, SUMOylation acts alongside the canonical chaperone-mediated feedback loop to ensure that HSF1 activity is transient. While the chaperone-mediated shut-down of HSF1 activity acts as a late feedback mechanism once a threshold of chaperone expression and availability is reached, we hypothesize that SUMOylation functions as a regulatory rheostat as soon as HSF1 is activated. In line with this hypothesis, SUMOylation occurs on the trimeric HSF1 following its activating phosphorylation [41]. We anticipate that this early feedback prepares cells for stress resolution and helps to avoid an overshooting of the stress response. Consistent with this idea, SUMOi exerts the

most pronounced inhibitory effects on highly inducible HSF1 targets, including *HSPA6* and *HSATIII*, that cluster multiple HSF1 binding sites.

Mechanistically, SUMOylation dampens HSF1 output by limiting co-activator engagement. We show that SUMO-deficient HSF1 displayed enhanced association with the general transcription machinery as well as transcriptional co-regulators and chromatin-remodelling factors. Notably, TADA3L, CRTC2 and the SWI/SNF subunit SMARCD3 were enriched in the HSF1 proximity network. TADA3L is associated with multiprotein complexes containing histone acetyltransferases such as GCN5/PCAF and p300/CBP, enabling cooperative recruitment of acetyltransferase activities, whereas CRTC2 functions as a co-activator of CREB/CBP-dependent transcription [46–53]. Although not previously linked to HSF1, their enhanced association, together with the sensitivity of HSF1 target gene expression to inhibition of p300/CBP, CREB–CRTC2 interaction, and SWI/SNF activity, suggests that multiple co-activator pathways act in concert to drive elevated transcription when SUMOylation is impaired. Interestingly, SWI/SNF complex has previously been shown to foster HSF1-driven gene expression [54,55] and its activity is SUMO dependent [56]. There is accumulating evidence that HSF1-driven transactivation occurs in transcriptional condensates that form via liquid-liquid phase separation at HSP gene loci [57]. The transient concentration of the transcription apparatuses within these condensates allows a rapid control of gene expression through dynamic condensate assembly and disassembly. Notably, the dynamics of HSF1 transcriptional condensates is regulated by phosphorylation within the intrinsically disordered region (IDR) of HSF1 [57]. Considering that K298 also resides within the IDR, it is tempting to speculate that SUMOylation exerts its inhibitory function on HSF1 by directly affecting condensate dynamics.

In support of this hypothesis, we demonstrated that SUMOylation of HSF1 is needed to properly disperse nSBs, which are a specific subtype of HSF1-driven transcriptional condensates forming at *HSATIII* loci. SUMO inhibition enhanced HSF1 binding at the HSATIII locus, increased *HSATIII* RNA levels and promoted the formation of enlarged and persistent nSBs. Expression of SUMO-deficient HSF1 phenocopied these effects, indicating that HSF1 SUMOylation directly controls nSB dynamics. Given that *HSATIII* RNA serves as a scaffold for nSB assembly, sustained HSF1 activity likely drives continued condensate formation. These findings align with emerging models in which stress-induced transcription occurs within dynamic condensates that must be actively disassembled during recovery. Persistent nSBs have important functional consequences for RNA metabolism. nSBs sequester RNA-processing factors and promote intron retention during recovery from heat shock [14]. Consistently, SUMO inhibition results in the increased sequestration of a group of splicing factors in nSBs along with a change in the intron retention landscape, indicating impaired restoration of normal splicing. Thus, SUMO-dependent attenuation of HSF1 activity coordinates the shutdown of canonical heat shock protein transcription with the recovery of RNA processing. Noteworthy, previous work has been identified K298 of HSF1 among the lysine residues targeted by p300-mediated acetylation [58]. Acetylation was shown to enhance HSF1 stability, thereby contributing to its activation cycle and pointing to a role of K298 as regulatory switchport for PTMs. In our study, however, chemical inhibition of SUMOylation as well as expression of the SUMO-deficient HSF1 variants that preserve K298, fully recapitulate the phenotypes observed with

the K298 variant, confirming that SUMOylation exerts a major regulatory role on the K298 residue of HSF1.

In summary, our findings support a model in which SUMO-2/3 conjugation to HSF1 functions as a molecular timer for stress recovery. By limiting co-activator engagement, restricting prolonged transcriptional competence, and enabling disassembly of nSBs, SUMOylation ensures timely attenuation of the HSR and restoration of cellular homeostasis. These results position SUMO signaling as a central component of the machinery that resets stress-induced gene expression programs following proteotoxic stress. Further, our work defines the disassembly of stress-induced molecular condensates as an overarching principle of SUMO signaling in stress recovery. The critical role of SUMO in dismantling nSBs mirrors our previous findings on SUMO-dependent disassembly of cytosolic SGs [27]. The data further illustrate that SUMO signaling integrates transcriptional, post-transcriptional and post-translational signaling to orchestrate chaperone- and UPS-controlled proteostasis networks [24]. Together, these observations underscore how SUMO reverts the stress-induced spatial compartmentalization of cellular activities within molecular condensates thereby contributing to the restoration of normal cell function.

Material & Methods

Cell culture and cell line generation

HeLa (female, ATCC CCL-2) cells were purchased from ATCC and cultured in Dulbecco's modified Eagle medium (DMEM) supplemented with 10% fetal calf serum (Gibco) and 1% penicillin–streptavidin mixture (10,000 U ml^{-1}; Gibco). HSF1 knock out (HSF1 KO) HeLa cell line was a gift from Prof. Dr. Christian Münch and was cultured in DMEM with 10% FCS supplementation. HeLa Flp in T-Rex™ cell line was transfected with indicated plasmids (in the background of pcDNA™5/FRT/TO) along with pOG44 Flp-Recombinase Expression Vector. Hygromycin was added (final concentration of 200µg/ml) 48 hours after transfection and the cells were kept under selection in Hygromycin-containing media until colonies start to appear. Transgene expression was induced by 12–16 hours of Doxycycline (1 µg/ml) exposure. Chemicals used in this study and added on the cells include TAK-981 (CT-TAK981; Chemietek), MG-132 (S2619; Selleckchem), KRIBB11 (HY-100872; MedChemExress), sodium arsenite (Sc-250986; Santa Cruz), Cadmium chloride (655198; Sigma-Aldrich), Biotin (B4639; Sigma-Aldrich), A-485 (HY-107455; MedChemExress), Artepillin C analog A57 (SML3449; Sigma-Aldrich), dBET6 (HY-112588; MedChemExress). GTPP (Shanghai Chempartner) and AU-15330 (MedChemExpress, HY-145388) were gifted by Prof. Dr. Christian Münch and Dr. Matthias S. Leisegang, respectively. Concentration and exposure time for the chemicals are indicated in the figure legends.

Transfection

Transfection of siRNA (Table S9) was carried out by Lipofectamine RNAiMAX reagent (Thermo Fisher Scientific) for 72 hours by following the manufacturer's instructions (reverse transfection method). *HSATIII* anti-sense oligo (*HSTAIII* ASO) was transfected by Lipofectamine™ 2000 Transfection Reagent

(Thermo Fischer Scientific) by following the manufacturer's instructions (forward transfection method) 16 hours before HS. Plasmid (list of plasmids were given in Table S10) transfection was carried out by FuGENE transfection reagent (Promega) for 24–48 hours as per the manufacturer's recommended protocol. FLAG-HSF1 was cut out from the Addgene plasmid #32537 (a gift from Stuart Calderwood; http://n2t.net/addgene:32537 ; RRID:Addgene_32537) [59] by *XhoI* and *HindIII* and inserted into the linearized (by *XhoI* and *HindIII*) recipient plasmid pcDNA5/FRT/TO to make pcDNA5/FRT/TO-FLAG-HSF1^{WT}. Further, pcDNA5/FRT/TO-FLAG-HSF1^{WT} was made siHSF1 resistant by two rounds of site-directed mutagenesis (SDM). Either addgene plasmid #32537 or siHSF1 resistant pcDNA5/FRT/TO-FLAG-HSF1^{WT} were further subjected to SDM to make the other (K-R, E-A) mutants. HSF1 (Addgene plasmid #32537) was inserted into the pDest53-HA-ultraID vector by SLIC cloning.

Immunoblot

For immunoblot analysis, protein samples were boiled in Laemmli buffer, subjected to SDS-PAGE, and were subsequently transferred on to Nitrocellulose membranes using wet blot technique in a Towbin buffer containing 20% methanol. Membranes were further blocked with 5% milk in PBS-T and probed overnight at 4°C with primary antibodies diluted in blocking buffer. Subsequently, the membranes were washed in PBS-T, and HRP coupled secondary antibodies diluted in blocking buffer were added for an hour at room temperature to the membranes. Finally, membranes were washed again with PBS-T and Immobilon Western Chemiluminescent HRP Substrate (Merck Millipore) was added to the membranes. Chemiluminescence signal was detected on a Bio-Rad ChemiDoc MP XRS+ imaging system. Lists of primary and secondary antibodies are given in Table S11.

Fractionation of cells into detergent (NP-40)-soluble and insoluble parts

Cells were treated as indicated, harvested in 1X PBS, and cell pellets were resuspended in NP-40 lysis buffer (25mM Tris-HCl; pH8.5, 150mM NaCl, 1% NP-40, 1mM EDTA, 20mM NEM, 50µM PR-619) supplemented with 1X cOmplete™ Protease Inhibitor Cocktail (Roche). After 30 mins of incubation on ice with intermittent vortexing, cell lysates were centrifuged at 20000g for 20 mins at 4^0C. Supernatants were collected as NP-40 soluble fractions and the pellets were further washed twice with 1XPBS, and finally lysed in SDS lysis buffer (2% SDS, 50mM Tris-HCl; pH 8.5, 10mM TCEP, 40mM CAA) supplemented with 1X cOmplete™ Protease Inhibitor Cocktail (Roche).

Quantitative Real Time PCR

Cells were treated as indicated and harvested by trypsinization. After washing off Trypsin with 1XPBS, total RNA was extracted with High Pure RNA isolation kit (Roche) and 500ng RNA was reverse transcribed by RNA to cDNA EcoDry™ Premix (Random Hexamers) or RNA to cDNA EcoDry™ Premix (Oligo dT). qPCR was performed with qPCR SYBRGreen Master Mix (Steinbrenner) and KiCqStart™ Primers (Merck) using the LightCycler 480 II (Roche). GAPDH gene expression was used for normalization. The Delta-Delta Ct ($2^{-\Delta\Delta Ct}$) method was applied for the determination of respective mRNA

expression. Three independent experiments were performed in technical quadruplicate. Primers are listed in Table S12.

Ni-NTA pull down

Purification of His-SUMO-2 conjugates on magnetic Ni-NTA beads (Qiagen) was performed as described previously [60]. In brief, cells were transfected with His-SUMO-2 alone or co-transfected as indicated. Cells were lysed in Ni-NTA-pull-down lysis buffer (6 M guanidine–HCl, 100mM NaH_2PO4, 0.05% Tween-20 and 100mM Tris–HCl (pH 8.0)), and His-SUMO-2 conjugates were purified on Ni-NTA beads which were then and boiled in Laemmli buffer for 10 mins.

Whole cell proteome, NP-40 soluble and insoluble proteome

Sample preparation: For whole cell proteome, Hela cells were lysed, reduced and alkylated in SDS lysis Buffer (2% SDS, 50mM Tris pH 8.5, 10mM TCEP, 40mM CAA) complemented with protease inhibitor tablet. For NP-40 soluble and insoluble proteome, cells were fractionated as described before. Insoluble pellets were resuspended directly in SDS lysis Buffer. NP-40 soluble fraction was mixed with SDS (final concentration 2%), CAA (final concentration 40mM), and TCEP (final concentration 10mM). Cellular lysates were subsequently boiled, sonicated and subjected to methanol-chloroform precipitation. The resulting dried pellet was resuspended in urea digestion buffer (8M urea, 50mM Tris pH 8.2) and protein concentration was measured by BCA assay (23225, Thermo Fischer Scientific, PierceTM BCA Protein Assay Kit). 50 µg protein was digested by Trypsin (enzymes to protein ratio 1:100) and Lys-C (enzymes to protein ratio 1:50) overnight at 37^0C in 1M urea, 50mM Tris pH 8.5. Proteolytic cleavage was stopped by TFA (final concentration 1%) and peptides were subsequently desalted using tC18 Sep-Pak cartridges (WAT054960, Waters, Milford, USA). Subsequently, digested peptides were dissolved in 200 mM EPPS pH 8.2, 10% ACN buffer and peptide concentration was measured by micro-BCA assay (Micro BCA™ Protein Assay Kit, 23235, Thermo Fischer Scientific). 10µg of digested peptides were finally labelled with TMTpro reagents (peptides to TMT ratio 1:2.5) or TMTsixplex reagents (peptides to TMT ratio 1:2) (ThermoFisher Scientific) for 1 h at room temperature. Quenching of the labelling reaction was performed by hydroxylamine at a final concentration of 0.5% and equal amounts of TMT labelled samples were pooled followed by cleaning up using tC18 Sep-Pak cartridges.

High pH micro-flow fractionation

Peptides were fractionated using high-pH liquid-chromatography on a micro-flow HPLC (Dionex U3000 RSLC, ThermoFisher Scientific). 45µg of pooled and purified TMT labelled peptides resuspended in Solvent A (5mM ammonium-bicarbonate, 5%ACN) were separated on a C18 column (XSelect CSH, 1mm x 150mm, 3.5 µm particle size, Waters) using a multistep gradient from 3–60% Solvent B (100% ACN) over 65 minutes at a flow rate of 30 µl/min. Eluting peptides were collected every 43 seconds from minute 2 for 69 minutes into a total of 96 fractions, which were cross-concatenated into 16/24 fractions. Pooled fractions were evaporated to dryness and stored at -20°C until mass spectrometry analysis.

Mass spectrometry

Fractions were resuspended in LC-MS grade water containing 2% ACN and 0.1% TFA. Peptides were separated on an easy nLC 1200 (ThermoFisher Scientific) and a 35 cm long, 75µm ID fused-silica column, which has been packed in-house with 1.9 µm C18 particles (ReproSil-Pur, Dr. Maisch, Ammerbuch, Germany) and kept at 50°C using an integrated column oven (Sonation). HPLC solvents consisted of 0.1% Formic acid in water (Buffer A) and 0.1% Formic acid, 80% Acetonitrile in water (Buffer B). Peptides were eluted by a non-linear gradient from 7 to 40% B over 90 minutes, followed by a step-wise increase to 90% B in 6 minutes, which was held for another 9 minutes, and directly sprayed into a Fusion Lumos mass spectrometer equipped with a nanoFlex ion source (ThermoFisher Scientific) at a spray voltage of 2.3 kV. MS analysis was performed using a Top-Speed method (1.5s cycle time) with the RF lens at 30%. Full scan MS spectra (350–1400 m/z) were acquired at a resolution of 120,000 at m/z 200, a maximum injection time of 100 ms and an AGC target value of 4×10^5. MS2 scans were performed in the Ion trap (Rapid) using an isolation window of 0.7 Th, a maximum injection time of 50 ms and fragmented using CID with a collision energy of 35%. SPS-MS3 was performed on the 10 most intense MS2 fragment ions with an isolation window of 0.7 Th (MS1) and 2 m/z (MS2). Ions were fragmented using HCD with a normalized collision energy of 50 and analyzed in the Orbitrap with a resolution setting of 50,000 at m/z 200, scan range of 100–500 m/z, AGC target value of 1.5×10^5 and a maximum injection time of 86ms. Repeated sequencing of already acquired precursors was limited by setting a dynamic exclusion time of 45 seconds and 7 ppm.

Raw data analysis and statistical significance evaluation: Raw data analysis was done with Proteome Discoverer (v 2.4). SequenceHT node was selected for database searches. Human trypsin digested proteome (Homo sapiens SwissProt database [20531]) was used for protein identifications. Contaminants (MaxQuant “contamination.fasta”) were determined for quality control. TMTpro (K, + 304.207 Da) for TMT 16 plex at the N terminus and carbamidomethyl (+ 57.021 Da) at cysteine residues were set as fixed modifications. TMTpro (K, + 304.207 Da) for TMT 16 plex, and methionine oxidation (M, + 15.995 Da) as well as Acetyl (+ 42.011 Da) at the protein N terminus were set for dynamic modifications. Precursor mass tolerance was set to 7 ppm and fragment mass tolerance was set to 0.02 Da. Default Percolator settings in PD were used to filter perfect spectrum matches (PSMs). Reporter ion quantification was achieved with default settings in consensus workflow. Peptide groups file was exported into .txt file and subsequent statistical analysis was done with the Perseus software (version 1.6.15.0). Log2 values of all the normalized abundances were calculated. Using the histogram analysis function of the software, the normal distribution of the abundance values was visually checked. Good correlation of the experimental replicates was assured by multi-scatterplot analysis. Samples were then grouped into triplicates and a Student’s t-test was performed with randomization of 250 and permutation-based FDR 0.05. Then the datasets were exported and used for further analysis in Microsoft Excel. Significant enrichment was defined in Excel based on the *P*-value and the Student’s t-test difference (mentioned in the figure legends). Visual representation of data in volcano plots was done R

Studio. Enrichment of gene ontology signatures was performed on an online portal ShinyGO v0.75: Gene Ontology Enrichment Analysis.

Proximity proteomics (ultraID)

Sample preparation

HeLa cells (HSF1 WT or HSF1 KO) were transfected with 3XHA-ultraID-HSF1 (WT or K298R) or empty vector (3XHA-ultraID) as indicated in the figure legends. 24 hours after transfection, cells were primed with SUMOi (200nM for 1 hour)/DMSO and were further given HS for another hour or kept under non-HS condition. 10 mins before HS, cells were treated with 50µM Biotin/DMSO. Finally, cells were harvested in 1X PBS and lysed in ultraID lysis buffer (50mM Tris pH 8.5, 0.1% SDS, 0.5% sodium deoxycholate, 1mM EDTA, 150mM NaCl, 1% Triton-X-100, 20mM NEM) supplemented with 1X cOmplete™ Protease Inhibitor Cocktail (Roche). After 20 mins of incubation on ice with intermittent vortexing, cell lysates were sonicated, centrifuged at 20000xg for 20 mins at 4^0C, and the supernatants were transferred to fresh tubes. Lowry assay was used to measure the protein concentration and 1mg of lysates were rotated overnight at 4^0C on NeutrAvidin agarose beads (Thermo Fischer Scientific). The beads were finally washed 4 times with ultraID wash buffer (50mM Tris pH8.5, 0.5% sodium deoxycholate, 1mM EDTA, 150mM NaCl, 1% Triton-X-100, 1% SDS, 20mM NEM) supplemented with 1X cOmplete™ Protease Inhibitor Cocktail (Roche), 2 times with 1X PBS followed by another 2 washes with 50mM Tris pH8.5. Elution was done with 2% SDC buffer (2% sodium deoxycholate, 1mM TCEP, 4mM CAA in 50mM Tris pH8.5) in dark at 96^0C on a thermomixer for 10 mins. Subsequently, overnight trypsin digestion (0.5ug Trypsin in 50mM Tris pH8.5) was set up for the eluted samples at 37^0C in a thermomixer. Trypsin digestion was stopped with 1% TFA in isopropanol, peptides were cleaned up on SDB-RPS, and dried peptides were stored at -20^0C until the MS run.

Mass spectrometry

Dried peptides were resuspended in 2% ACN with 0.1% TFA prior to LC-MS/MS analysis on an Orbitrap Lumos coupled to an easy nLC 1200 (ThermoFisher Scientific) using a 35 cm long, 75µm ID fused-silica column packed in house with 1.9 µm C18 particles (Reprosil pur, Dr. Maisch), and kept at 50°C using an integrated column oven (Sonation). HPLC solvents consisted of 0.1% Formic acid in water (Buffer A) and 0.1% Formic acid, 80% acetonitrile in water (Buffer B). Peptides were eluted in a non-linear gradient of 4–35% Buffer B over 60 min followed by a step-wise increase to 95% Buffer B in 6 minutes, which was held for another 9 minutes and directly sprayed into the mass spectrometer equipped with a nanoFlex ion source (Thermo Fisher Scientific). Full-scan MS spectra (300–1,500 m/z) were acquired in profile mode at a resolution of 60,000 at m/z 200, a maximum injection time of 50 ms and an automatic gain control (AGC) target of 4×10^5. Up to 10 of the most intense peptides per full scan were isolated using a 1.4-Th window for fragmentation by higher energy collisional dissociation (normalized collision energy of 30). MS/MS spectra were acquired in centroid mode with a resolution of 30,000, a maximum injection time of

54 ms and an AGC target value of 1×10^5. Only ions with a charge state between 2 and 6 were considered for fragmentation.

Raw data analysis and statistical significance evaluation: MS raw data were analyzed using FragPipe v22.0, with MSFragger v.4.1 [61] and Philosopher v.5.1.1. [62]. The built-in workflow "LFQ-MBR" was used with a precursor mass tolerance of 20 ppm and fragment mass tolerance of 20 ppm. The human proteome database (ID: UP000005640, 07/08/2024) used for the search encompassed 20,467 reviewed sequences and their corresponding decoys, including common contaminant proteins. Identifications were filtered to obtain false discovery rates (FDR) below 1% for both peptide spectrum matches (minimum peptide length of 7) and proteins using a target-decoy strategy. For all searches, carbamidomethylated cysteine was set as a fixed modification and oxidation of methionine, N-terminal protein acetylation, allowing up to 3 modifications per peptide. Strict trypsin cleavage was set as the protein digestion rule. Label-free quantification was performed using IonQuant v.1.10.27 [63]. The Data were further processed using FragPipe Analyst [64]. Proteins that were identified in in 2 out of 3 replicates in at least one condition were kept, while proteins that were only present in one replicate per condition were filtered out prior to Perseus-type imputation. After imputation, differential expression analysis was performed using Limma and p-values were corrected by Benjamini-Hochberg for multiple comparisons.

Confocal microscopy

Cells grown on 12-mm glass coverslips were treated as indicated, washed with 1X PBS, and fixed in 4% paraformaldehyde (PFA) for 15 minutes at room temperature. After 3 washes with 1x PBS, cells were permeabilized with 0.3% Triton-X-100 in 1X PBS and blocked with 3% BSA for 1 h at room temperature. Primary antibodies were diluted in antibody dilution buffer (1% BSA, 0.1% TritonX100 in 1x PBS) according to manufacturer's recommendations and incubated overnight at 4°C in a moist chamber. After three washes with antibody dilution buffer, secondary antibody (anti-rabbit Alexa 488) was added and incubated for 1 h at 37°C in a moist chamber. The cells were washed three times with 1X PBS followed by staining with the nuclear stain DAPI for 10 min. Finally, the cells were washed once with 1x PBS before mounting with Fluoromount-G. Slides were imaged using a Leica SP8 confocal microscope fitted with a ×63 oil-immersion lens and analysed with ImageJ software (version 1.51w).

RNA sequencing and analysis

Total RNA was isolated using the High Pure RNA isolation kit (Roche). Quality and amount were checked using TapeStation RNA (Agilent) and Qubit (Invitrogen). Processing, library generation and paired-end sequencing (150 bp/read) of RNA samples has been performed by Novogene (Cambridge, UK). Paired-end RNA sequencing reads were aligned to the human reference genome GRCh38/hg38 using STAR (v2.7.11b) [65]. The genome index was generated from the hg38 primary assembly together with the GENCODE comprehensive gene annotation (release 46; Ensembl 112). Alignments were performed in splice-aware mode and written as coordinate-sorted BAM files. Gene-level read quantification was performed using HTSeq-count [66] based on the GENCODE annotation. Raw count matrices were analyzed in R using DESeq2 [67]. Genes with low counts were filtered prior to analysis. Differential expression was

assessed using pairwise comparisons between experimental conditions, and significance thresholds were defined as adjusted *P* value (Benjamini-Hochberg correction) and log2 fold change.

Functional enrichment analysis was performed using GeneTrail3 [68], executed as a local installation on a high-performance computing (HPC) environment. The GeneTrail3 source code is available at:

https://github.com/unisb-bioinf/genetrail3 . Ranked gene lists derived from differential expression analyses were used as input for pathway enrichment. Gene identifiers were converted to gene symbols where required, and enrichment analysis was performed using curated pathway collections (e.g., Reactome, GO). Statistical significance was assessed using GeneTrail's internal enrichment framework with multiple-testing correction (Benjamini-Hochberg).

CUT&RUN

CUT&RUN assays were performed on HeLa cells using the CUT&RUN Assay Kit (Cell Signaling Technology, Cat. No. 86652) according to the manufacturer's instructions. Briefly, 100,000 cells were seeded and, the following day, treated with 200 nM TAK981 or DMSO for 1 hour, followed by a 1-hour heat shock at 42–43°C. Cells were then harvested following the manufacturer's protocol and bound to previously activated Concanavalin A-coated magnetic beads. The bead-cell complex was permeabilized with digitonin and incubated overnight at 4°C with the appropriate primary antibody. Antibodies used for chromatin precipitation included those targeting HSF1, along with an IgG control. After antibody binding, complexes were washed and incubated with protein A/G-micrococcal nuclease (pAG/MNase). Chromatin digestion was initiated by calcium chloride addition and incubation at 4°C for 30 minutes, and the reaction was stopped by incubating in the stop buffer at 37°C for 10 minutes to release the fragments. For input samples, chromatin was sonicated for 17 cycles (30" on/30" off) to obtain DNA fragments of 100–600 base pairs. Fragment size was confirmed on 1.5% agarose gel. DNA fragments were purified using DNA Purification Buffers and Spin Column (Cell Signaling Technology, Cat No. 14209). DNA concentrations were determined using Qubit 2.0 Fluorometer (Thermo Fischer Scientific, Cat. No. Q32866) and Qubit dsDNA HS Assay Kit (Thermo Fischer Scientific, Cat. No. 32854).

For next-generation sequencing (NGS), CUT&RUN purified DNA (2.5–10 ng) was used to generate sequencing libraries using the DNA Library Prep Kit for Illumina (Cell Signaling Technology, ChIP-seq, CUT&RUN; Cat. No. 56795) and Multiplex Oligos for Illumina Systems (Cell Signaling Technology, Dual Index Primers, ChIP-seq, CUT&RUN, Cat. No. 47538) according to the manufacturer's instructions. In brief, DNA was end-repaired and A-tailed, ligated to Illumina adaptors containing unique indexes, and amplified for 9–17 cycles depending on the initial DNA concentration. Libraries were purified, and double-size selection was performed using NucleoMag magnetic beads (Macherey- Nagel, Cat. No. 744970.50) to enrich DNA fragments of 200–400 base pairs according to the manufacturer's instructions. Library quality and fragment size distribution were assessed by capillary electrophoresis (Bioanalyzer 2100, Agilent Technologies). Prepared libraries were sent to Novogene (Munich, Germany) for paired-end sequencing on an Illumina NovoSeq platform.

CUT&RUN sequencing reads for HSF1 were aligned to the human reference genome GRCh38/hg38 using Bowtie2 (v2.5.4) [69] with parameters optimized for sensitive local alignment (--very-sensitive-local, --no-mixed, --no-discordant). Alignments were sorted and indexed using SAMtools [70], and quality metrics were assessed using standard alignment statistics.

Genome-wide HSF1 binding sites were identified using MACS2 [71] in paired-end mode (BAMPE) with a genome size parameter corresponding to human (-g hs) and a false discovery rate threshold of $q < 0.01$. Biological replicates were analyzed individually and as pooled datasets to increase sensitivity.

To investigate HSF1 occupancy at *HSATIII* loci, CUT&RUN data were additionally analyzed in the hs1/CHM13v2 reference framework [72], which provides improved representation of satellite sequences. Reads were evaluated relative to curated *HSATIII* interval annotations using BEDTools [73], enabling locus-specific quantification of HSF1 enrichment at satellite III regions. This complementary analysis captures binding events in repetitive genomic regions not resolved in hg38-based peak calling.

Genome-wide signal tracks were generated from aligned BAM files using deepTools (v3.x) [74]. Normalized coverage files were computed using bamCoverage with normalization to reads per kilobase per million mapped reads (RPKM) or counts per million (CPM), as appropriate. Signal enrichment profiles and heatmaps centered on peak summits or transcription start sites were generated using computeMatrix followed by plotHeatmap or plotProfile. These analyses enabled comparative visualization of CUT&RUN signal intensities across conditions and genomic regions.

Sequence motif enrichment within CUT&RUN peaks was performed using the MEME Suite (including MEME-ChIP) [75]. For this analysis, peak regions were mapped to the hg19 reference genome, which is the default coordinate framework for several MEME Suite-associated regulatory tools. To associate distal binding sites with putative target genes, T-Gene (part of the MEME Suite) was used [75]. T-Gene integrates genomic proximity and regulatory potential to assign transcription factor binding sites to likely target genes. CUT&RUN peak coordinates were analyzed in the hg19 reference framework for compatibility with the T-Gene algorithm and associated annotation resources.

RNA-seq and intron retention

Total RNA was isolated using the High Pure RNA isolation kit (Roche). Quality and amount were checked using TapeStation RNA (Agilent) and Qubit (Invitrogen). Processing, library generation and paired-end sequencing (150 bp/read) of RNA samples has been performed by Novogene (Cambridge, UK). For differential intron retention analysis, the raw, demultiplexed files were aligned to the GRCh19.p14 genome assembly using STAR v.2.7.11b [65]. The resulting .bam files with aligned reads were used as input for IRFinder-S v.2.0.1 [76] in DESeq2 mode. Introns exhibiting significant changes in retention were identified using a p-value threshold of < 0.05. Differentially retained introns were classified as up- or downregulated based on their ΔPSI (Percent-spliced-in) values. Conservation scores were retrieved from

the pre-computed 100-vertebrate phastCons track provided in the R package phastCons100way.UCSC.hg38 [77].

Declarations

Acknowledgements

We thank all members of the Centre for Functional Proteomics (Goethe University, Frankfurt), particularly Martin Adrian-Allgood. This work was supported by Deutsche Forschungsgemeinschaft (DFG grants MU-1764/6- Project ID-465470262, MU-1764/7- Project ID- 494535244, MU-1764/6- Project ID-571860567, CRC387, Project-ID 514894665, Germany´s Excellence Strategy – EXC-3094–533751785 to S.M. and FuGG Project-ID: 403765277 that funded the LC-MS system (easy nLC1200, Orbitrap Fusion LUMOS), the BMBF Project: "PROXIDRUGS" funded by the German Federal Ministry of Education and Research to S.M.

Data availability

The mass spectrometry data have been deposited to the ProteomeXchange Consortium via the PRIDE [78] partner repository with the dataset identifiers PXD077087, PXD077128, PXD077148, PXD077164, PXD077181, PXD077194, PXD077245. The RNAseq and CUT&RUN data have been deposited to the European Nucleotide Archive (Accession ID: PRJEB111743).

Declaration of generative AI and AI-assisted technologies in the manuscript preparation process

During the preparation of this work the author(s) used ChatGtP in order to correct language and grammar of this manuscript. After using this tool/service, the author(s) reviewed and edited the content as needed and take full responsibility for the content of the published article.

References

1. Hipp MS, Hartl FU (2024) Interplay of Proteostasis Capacity and Protein Aggregation: Implications for Cellular Function and Disease. J Mol Biol 436:168615
2. Labbadia J, Morimoto RI (2015) The biology of proteostasis in aging and disease. Annu Rev Biochem 84:435–464
3. Kuzu OF, Granerud LJT, Saatcioglu F (2025) Navigating the landscape of protein folding and proteostasis: from molecular chaperones to therapeutic innovations. Signal Transduct Target Ther 10:358
4. Amzallag E, Hornstein E (2022) Crosstalk between Biomolecular Condensates and Proteostasis. *Cells* 11
5. Biamonti G (2010) Vourc'h, C. Nuclear stress bodies. Cold Spring Harb Perspect Biol 2:a000695

6. Goenka A et al (2016) Human satellite-III non-coding RNAs modulate heat-shock-induced transcriptional repression. J Cell Sci 129:3541–3552
7. Akerfelt M, Morimoto RI, Sistonen L (2010) Heat shock factors: integrators of cell stress, development and lifespan. Nat Rev Mol Cell Biol 11:545–555
8. Gomez-Pastor R, Burchfiel ET, Thiele DJ (2018) Regulation of heat shock transcription factors and their roles in physiology and disease. Nat Rev Mol Cell Biol 19:4–19
9. Kmiecik SW, Mayer MP (2022) Molecular mechanisms of heat shock factor 1 regulation. Trends Biochem Sci 47:218–234
10. Pessa JC, Joutsen J, Sistonen L (2024) Transcriptional reprogramming at the intersection of the heat shock response and proteostasis. Mol Cell 84:80–93
11. Chowdhary S, Kainth AS, Paracha S, Gross DS, Pincus D (2022) Inducible transcriptional condensates drive 3D genome reorganization in the heat shock response. Mol Cell 82:4386–4399e7
12. Fujimoto M, Takii R, Nakai A (2023) Regulation of HSF1 transcriptional complexes under proteotoxic stress: Mechanisms of heat shock gene transcription involve the stress-induced HSF1 complex formation, changes in chromatin states, and formation of phase-separated condensates: Mechanisms of heat shock gene transcription involve the stress-induced HSF1 complex formation, changes in chromatin states, and formation of phase-separated condensates. BioEssays 45:e2300036
13. Okada M et al (2023) The Mediator subunit MED12 promotes formation of HSF1 condensates on heat shock response element arrays in heat-shocked cells. FEBS Lett 597:1702–1717
14. Ninomiya K et al (2020) LncRNA-dependent nuclear stress bodies promote intron retention through SR protein phosphorylation. EMBO J 39:e102729
15. Ninomiya K et al (2021) m(6) A modification of HSATIII lncRNAs regulates temperature-dependent splicing. EMBO J 40:e107976
16. Golebiowski F et al (2009) System-wide changes to SUMO modifications in response to heat shock. Sci Signal 2:ra24
17. Seifert A, Schofield P, Barton GJ, Hay RT (2015) Proteotoxic stress reprograms the chromatin landscape of SUMO modification. Sci Signal 8:rs7
18. Tatham MH, Matic I, Mann M, Hay RT (2011) Comparative proteomic analysis identifies a role for SUMO in protein quality control. Sci Signal 4:rs4
19. Niskanen EA et al (2015) Global SUMOylation on active chromatin is an acute heat stress response restricting transcription. Genome Biol 16:153
20. Cappadocia L, Lima CD (2018) Ubiquitin-like Protein Conjugation: Structures, Chemistry, and Mechanism. Chem Rev 118:889–918
21. Vertegaal ACO (2022) Signalling mechanisms and cellular functions of SUMO. Nat Rev Mol Cell Biol 23:715–731

22. Oh E, Akopian D, Rape M (2018) Principles of Ubiquitin-Dependent Signaling. Annu Rev Cell Dev Biol 34:137–162
23. Gwon Y et al (2021) Ubiquitination of G3BP1 mediates stress granule disassembly in a context-specific manner. Science 372:eabf6548
24. Liebelt F et al (2019) SUMOylation and the HSF1-Regulated Chaperone Network Converge to Promote Proteostasis in Response to Heat Shock. *Cell Rep* 26, 236–249 e4
25. Wang W, Matunis MJ (2023) Paralogue-Specific Roles of SUMO1 and SUMO2/3 in Protein Quality Control and Associated Diseases. Cells 13
26. Guo L et al (2014) A cellular system that degrades misfolded proteins and protects against neurodegeneration. Mol Cell 55:15–30
27. Keiten-Schmitz J et al (2020) The Nuclear SUMO-Targeted Ubiquitin Quality Control Network Regulates the Dynamics of Cytoplasmic Stress Granules. Mol Cell 79:54–67e7
28. Gotthardt G, Keiten-Schmitz J, Muller S (2025) Reprogramming SUMO-primed ubiquitylation: opportunities in oncology and neurology. Trends Pharmacol Sci 46:1117–1129
29. Jansen NS, Vertegaal ACO (2021) A Chain of Events: Regulating Target Proteins by SUMO Polymers. Trends Biochem Sci 46:113–123
30. Maxwell BA et al (2021) Ubiquitination is essential for recovery of cellular activities after heat shock. Science 372:eabc3593
31. Kumar R, Gonzalez-Prieto R, Xiao Z, Verlaan-de Vries M, Vertegaal AC (2017) O. The STUbL RNF4 regulates protein group SUMOylation by targeting the SUMO conjugation machinery. Nat Commun 8:1809
32. Sui X et al (2020) Widespread remodeling of proteome solubility in response to different protein homeostasis stresses. Proc Natl Acad Sci U S A 117:2422–2431
33. Sutandy FXR, Gossner I, Tascher G, Munch C (2023) A cytosolic surveillance mechanism activates the mitochondrial UPR. Nature 618:849–854
34. Yoon YJ et al (2011) KRIBB11 inhibits HSP70 synthesis through inhibition of heat shock factor 1 function by impairing the recruitment of positive transcription elongation factor b to the hsp70 promoter. J Biol Chem 286:1737–1747
35. Heynen G et al (2023) SUMOylation inhibition overcomes proteasome inhibitor resistance in multiple myeloma. Blood Adv 7:469–481
36. Bardelcik M et al (2025) SUMOylation is not a prerequisite for HSF1's role in stress protection and transactivation. Sci Rep 15:24077
37. Hietakangas V et al (2006) PDSM, a motif for phosphorylation-dependent SUMO modification. Proc Natl Acad Sci U S A 103:45–50
38. Hong Y et al (2001) Regulation of heat shock transcription factor 1 by stress-induced SUMO-1 modification. J Biol Chem 276:40263–40267

39. Hendriks IA et al (2014) Uncovering global SUMOylation signaling networks in a site-specific manner. Nat Struct Mol Biol 21:927–936
40. Hendriks IA, Vertegaal AC (2016) A comprehensive compilation of SUMO proteomics. Nat Rev Mol Cell Biol 17:581–595
41. Kmiecik SW, Drzewicka K, Melchior F, Mayer MP (2021) Heat shock transcription factor 1 is SUMOylated in the activated trimeric state. J Biol Chem 296:100324
42. Burchfiel ET, Vihervaara A, Guertin MJ, Gomez-Pastor R, Thiele DJ (2021) Comparative interactomes of HSF1 in stress and disease reveal a role for CTCF in HSF1-mediated gene regulation. J Biol Chem 296:100097
43. Fujimoto M et al (2022) HSF1 phosphorylation establishes an active chromatin state via the TRRAP-TIP60 complex and promotes tumorigenesis. Nat Commun 13:4355
44. Boutz PL, Bhutkar A, Sharp PA (2015) Detained introns are a novel, widespread class of post-transcriptionally spliced introns. Genes Dev 29:63–80
45. Zhang B, Fan Y, Tan K (2025) HSF1 Activation Mechanisms, Disease Roles, and Small Molecule Therapeutics. Int J Biol Sci 21:3351–3378
46. Altarejos JY, Montminy M (2011) CREB and the CRTC co-activators: sensors for hormonal and metabolic signals. Nat Rev Mol Cell Biol 12:141–151
47. Berger SL (1999) Gene activation by histone and factor acetyltransferases. Curr Opin Cell Biol 11:336–341
48. Conkright MD et al (2003) TORCs: transducers of regulated CREB activity. Mol Cell 12:413–423
49. Dentin R et al (2007) Insulin modulates gluconeogenesis by inhibition of the coactivator TORC2. Nature 449:366–369
50. Koo SH et al (2005) The CREB coactivator TORC2 is a key regulator of fasting glucose metabolism. Nature 437:1109–1111
51. Ogryzko VV et al (1998) Histone-like TAFs within the PCAF histone acetylase complex. Cell 94:35–44
52. Wang T et al (2001) hADA3 is required for p53 activity. EMBO J 20:6404–6413
53. Watling KJ, Aspley S, Swain CJ, Saunders J (1988) [3H]quaternised ICS 205–930 labels 5-HT3 receptor binding sites in rat brain. Eur J Pharmacol 149:397–398
54. Lyu X, Rowley MJ, Corces VG (2018) Architectural Proteins and Pluripotency Factors Cooperate to Orchestrate the Transcriptional Response of hESCs to Temperature Stress. *Mol Cell* 71, 940–955 e7
55. Sullivan EK, Weirich CS, Guyon JR, Sif S, Kingston RE (2001) Transcriptional activation domains of human heat shock factor 1 recruit human SWI/SNF. Mol Cell Biol 21:5826–5837
56. Floros KV et al (2025) Targeting SUMOylation promotes cBAF complex stabilization and disruption of the SS18::SSX transcriptome in synovial sarcoma. Nat Commun 16:9761
57. Zhang H et al (2022) Reversible phase separation of HSF1 is required for an acute transcriptional response during heat shock. Nat Cell Biol 24:340–352

58. Raychaudhuri S et al (2014) Interplay of acetyltransferase EP300 and the proteasome system in regulating heat shock transcription factor 1. *Cell* 156, 975 – 85
59. Wang X, Grammatikakis N, Siganou A, Calderwood SK (2003) Regulation of molecular chaperone gene transcription involves the serine phosphorylation, 14-3-3 epsilon binding, and cytoplasmic sequestration of heat shock factor 1. Mol Cell Biol 23:6013–6026
60. Muller S et al (2000) c-Jun and p53 activity is modulated by SUMO-1 modification. J Biol Chem 275:13321–13329
61. Kong AT, Leprevost FV, Avtonomov DM, Mellacheruvu D, Nesvizhskii AI (2017) MSFragger: ultrafast and comprehensive peptide identification in mass spectrometry-based proteomics. Nat Methods 14:513–520
62. da Leprevost V (2020) Philosopher: a versatile toolkit for shotgun proteomics data analysis. Nat Methods 17:869–870
63. Yu F, Haynes SE, Nesvizhskii AI (2021) IonQuant Enables Accurate and Sensitive Label-Free Quantification With FDR-Controlled Match-Between-Runs. Mol Cell Proteom 20:100077
64. Hsiao Y et al (2024) Analysis and Visualization of Quantitative Proteomics Data Using FragPipe-Analyst. J Proteome Res 23:4303–4315
65. Dobin A et al (2013) STAR: ultrafast universal RNA-seq aligner. Bioinformatics 29:15–21
66. Anders S, Pyl PT, Huber W (2015) HTSeq–a Python framework to work with high-throughput sequencing data. Bioinformatics 31:166–169
67. Love MI, Huber W, Anders S (2014) Moderated estimation of fold change and dispersion for RNA-seq data with DESeq2. Genome Biol 15:550
68. Gerstner N et al (2020) GeneTrail 3: advanced high-throughput enrichment analysis. Nucleic Acids Res 48:W515–W520
69. Langmead B, Salzberg SL (2012) Fast gapped-read alignment with Bowtie 2. Nat Methods 9:357–359
70. Li H et al (2009) The Sequence Alignment/Map format and SAMtools. Bioinformatics 25:2078–2079
71. Zhang Y et al (2008) Model-based analysis of ChIP-Seq (MACS). Genome Biol 9:R137
72. Nurk S et al (2022) The complete sequence of a human genome. Science 376:44–53
73. Quinlan AR, Hall IM (2010) BEDTools: a flexible suite of utilities for comparing genomic features. Bioinformatics 26:841–842
74. Ramirez F et al (2016) deepTools2: a next generation web server for deep-sequencing data analysis. Nucleic Acids Res 44:W160–W165
75. Bailey TL, Johnson J, Grant CE, Noble WS (2015) The MEME Suite. Nucleic Acids Res 43:W39–49
76. Lorenzi C et al (2021) IRFinder-S: a comprehensive suite to discover and explore intron retention. Genome Biol 22:307
77. Siepel A et al (2005) Evolutionarily conserved elements in vertebrate, insect, worm, and yeast genomes. Genome Res 15:1034–1050

78. Perez-Riverol Y et al (2025) The PRIDE database at 20 years: 2025 update. Nucleic Acids Res 53:D543–D553

Figures

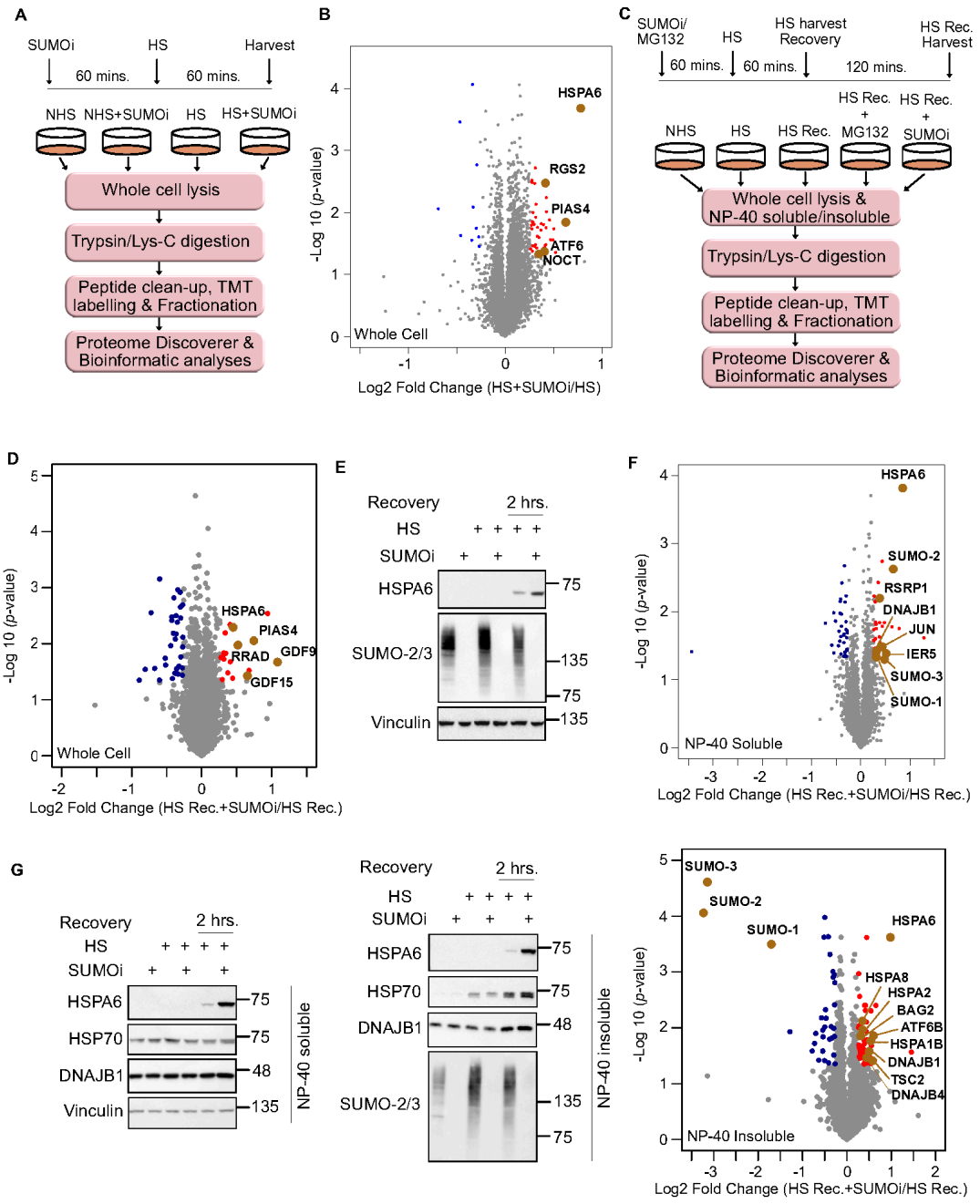

Figure 1

Figure 1

SUMO signaling reshapes stress-regulated cellular proteome. (A) Schematic representation of the TMT-based quantitative whole cell proteomics workflow of control (non-heat shock) and heat-shocked HeLa cells pre-primed with either DMSO or SUMOi (TAK-981; 200nM). **(B)** Volcano plot showing the relative fold change (Log2 scale) of proteins in the HS+SUMOi group compared to the only HS (HS+DMSO) group (data is obtained from the proteomics experiment described in a). *P*-values for the fold change (represented in the -Log10 scale in the y-axis) were calculated by Paired Student's t test (n=3). Significantly enriched (Log2 fold change>0.263; -Log10 *p*-value>1.34) and depleted proteins (Log2 fold change<0.263; -Log10 *p* value>1.34) were coloured red and blue, respectively. Relevant proteins are highlighted and labelled. **(C)** Schematic representation of the TMT-based quantitative whole cell as well as NP-40 soluble/insoluble proteomics workflow of control (non-heat shock), heat-shocked, and HS-recovered (HS Rec.) HeLa cells were pre-primed with DMSO/SUMOi (TAK-981; 200nM)/MG-132 (10 μM). **(D)** Volcano plot showing the relative fold change (Log2 scale) of proteins in the HS Rec.+SUMOi group compared to the only HS Rec. (HS rec.+DMSO) group (data is obtained from the proteomics experiment described in c). *P*-values for the fold change (represented in the -Log10 scale in the y-axis) were calculated by Paired Student's t test (n=3). Significantly enriched (Log2 fold change>0.263; -Log10 *p* value>1.34) and depleted proteins (Log2 fold change<0.263; -Log10 *p* value>1.34) were coloured red and blue, respectively. Relevant proteins are highlighted and labelled. **(E)** Western blot showing the whole cell protein levels of HSPA6, SUMO-2/3, and Vinculin (used as the internal loading control) in control (non-heat shock), heat-shocked (1 h), and heat shock-recovered (2 h) HeLa cells in presence of DMSO/SUMOi (200 nM; treated 1 h before HS). **(F)** Volcano plot showing the relative fold change (Log2 scale) of proteins in the HS Rec.+SUMOi group compared to the only HS Rec. (HS rec.+DMSO) group in both the NP-40 soluble and NP-insoluble fractions (data is obtained from the proteomics experiment described in c). *P*-values for the fold change (represented in the -Log10 scale in the y-axis) were calculated by Paired Student's t test (n=3). Significantly enriched (Log2 fold change>0.263; -Log10 *p*-value>1.34) and depleted proteins (Log2 fold change<0.263; -Log10 *p*-value>1.34) were coloured red and blue, respectively. Relevant proteins are highlighted and labelled. **(G)** Western blot showing the protein levels of HSPA6, HSP70, DNAJB1, SUMO-2/3, and Vinculin (used as the internal loading control in the NP-40 soluble fraction) in the NP-40 soluble and NP-40 insoluble fractions of control (non-heat shock), heat-shocked (1 h), and heat shock-recovered (2 h) HeLa cells in presence of DMSO/SUMOi (200 nM; added 1 h before HS).

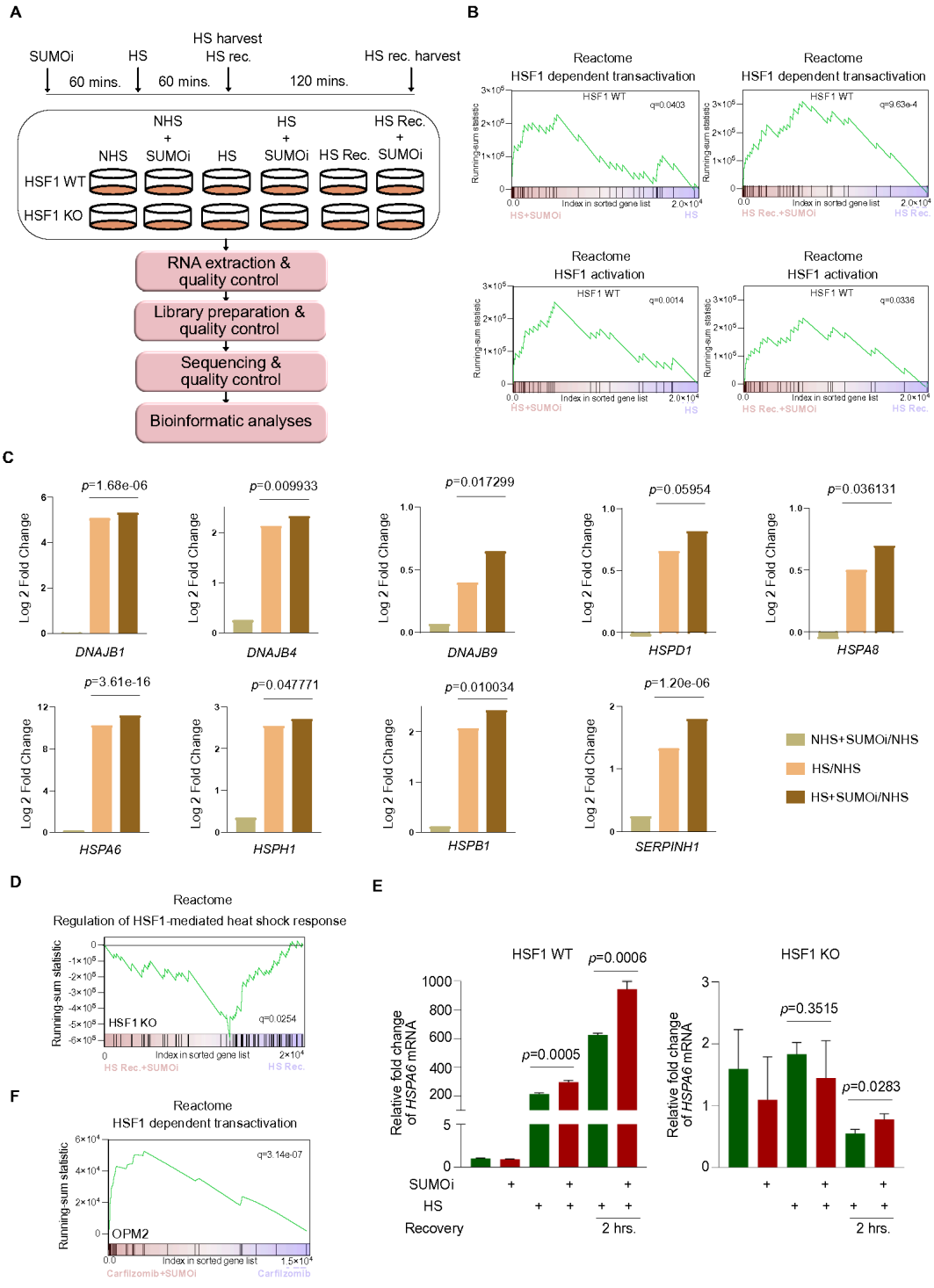

Figure 2

Figure 2

SUMOylation attenuates HSF1-driven gene expression programs. (A) Schematic representation of the RNAseq experimental workflow of control (non-heat shock), heat-shocked (1 h), and HS-recovered (2 h) HeLa cells that are either proficient (HeLa WT) or deficient of HSF1 (HSF1 KO) in presence of DMSO/SUMOi (200 nM; added 1 h before HS). **(B)** Gene set enrichment analysis based on curated Reactome annotations showing that genes belonging to the “HSF1 activation” and “HSF1-dependent

transactivation" pathways are significantly enriched in SUMOi-primed HeLa cells both during HS and HS recovery under HSF1 proficient condition. Adjusted *p* value is denoted by q. **(C)** Log2 fold changes of selected genes as obtained from the RNAseq data of HSF1 WT HeLa cells were represented. **(D)** Gene set enrichment analysis based on curated Reactome annotation showing genes belonging to the "Regulation of HSF1-mediated heat shock response" pathway being depleted in SUMOi-primed condition during HS recovery in HSF1 knock out HeLa cells. Adjusted *p* value is denoted by q. **(E)** HeLa cells were treated as indicated in Figure 2A; relative fold change of *HSPA6* mRNA was quantified by qPCR (normalized against *GAPDH* mRNA) in different treatment groups over the NHS control (NHS+DMSO). Results were shown as mean±standard deviation; *p* value was calculated based two-sided Student's t-tests (n=3). **(F)** OPM2 multiple myeloma cell line was subjected to single or combinatorial treatment of Carfilzomib and Subasumstat (SUMOi) (data obtained from (Heynen et al., 2023)). Gene set enrichment analysis based on curated Reactome annotations showing that genes belonging to the "HSF1-dependent transactivation" pathways are significantly enriched in SUMOi+Carfilzomib-primed cells compared to only Carfilzomib treatment. Adjusted *p* value is denoted by q.

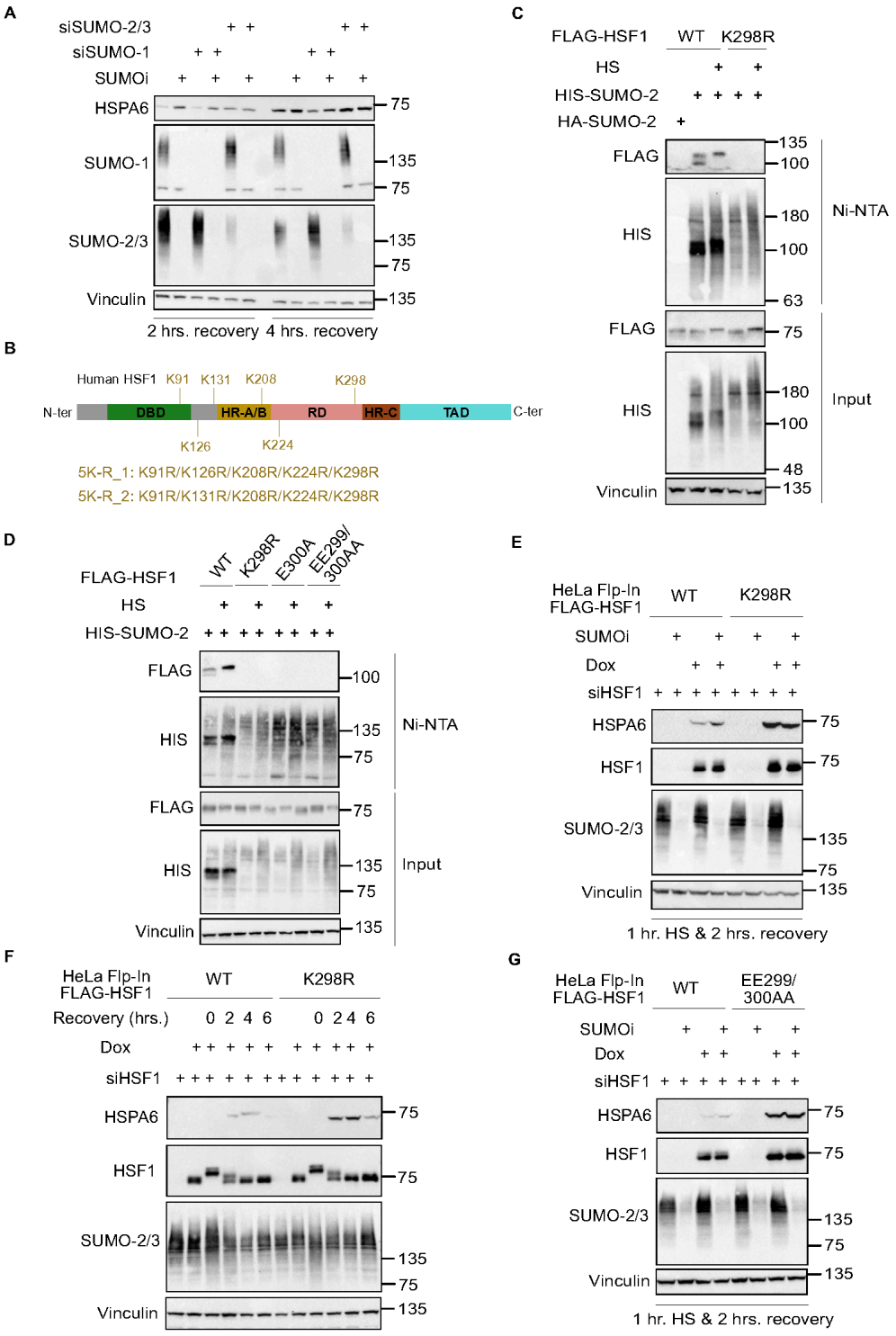

Figure 3

Figure 3

SUMO-2/3 conjugation to HSF1 controls the HSF1-driven proteotoxic stress response. (A) HeLa cells were reverse transfected with either siGL2, siSUMO-1, or siSUMO-2/3 for 72 hours and were further primed with DMSO/SUMOi (TAK-981, 200nM) for another hour. Subsequently, cells were heat-shocked (1 h) and allowed to recover (2 and 4 h) before cellular lysates were subjected to SDS-PAGE/immunoblotting for checking protein levels of HSPA6, SUMO-1, SUMO-2/3, and Vinculin. **(B)**

Domain structure of human HSF1; DBD: DNA binding domain, HR-A/B: Heptad repeat A/B, RD: Regulatory domain, HR-C: Heptad repeat C, TAD: Transactivation domain. High confidence SUMOylation (SUMO-2/3) sites are marked. **(C, D)** HeLa cells were transfected with HA-SUMO-2 or HIS-SUMO-2 and FLAG-HSF1 WT/K298R/E300A/EE299-300AA for 36 hours as indicated. One set of transfected cells was further heat-shocked (1 h). Subsequently, SUMO-2 conjugated fractions were enriched from the denatured cellular lysates on Ni-NTA magnetic beads and checked for the relative abundance of FLAG (HSF1) and HIS (SUMO-2) by SDS-PAGE/immunoblotting. 10% cellular lysates were subjected to TCA precipitation and used as “Input” to assess protein levels of FLAG (HSF1), HIS (SUMO-2), and Vinculin. **(E, G)** HeLa Flp-In FLAG-HSF1 WT (siHSF1-resistant) and **(E)** FLAG-HSF1^{K298R} (siHSF1-resistant)/**(G)**FLAG-HSF1$^{EE299-300AA}$ (siHSF1-resistant) cells were reverse transfected with siHSF1 and kept for 72 hours. Vehicle control or Doxycycline (1 µg/ml) was added for the last 16 hours of transfection. Cells were further treated with DMSO/SUMOi (TAK-981; 200 nM for 1 h), heat-shocked (1 h), and recovered (2 h) before the whole cell lysates were subjected to SDS-PAGE/immunoblotting for checking protein levels of HSPA6, HSF1, SUMO-2/3, and Vinculin. **(F)** HeLa Flp-In FLAG-HSF1 WT (siHSF1-resistant) and FLAG-HSF1^{K298R} (siHSF1-resistant) cells were reverse transfected with siHSF1 and kept for 72 hours. Vehicle control or Doxycycline (1 µg/ml) was added for the last 16 hours of transfection. Further, whole cell lysates were prepared at indicated time points (non-HS, HS for 1 h, and HS recovery for 2, 4 and 6 h), run on SDS-PAGE, and immunoblotted to check protein levels of HSPA6, HSF1, SUMO-2/3, and Vinculin.

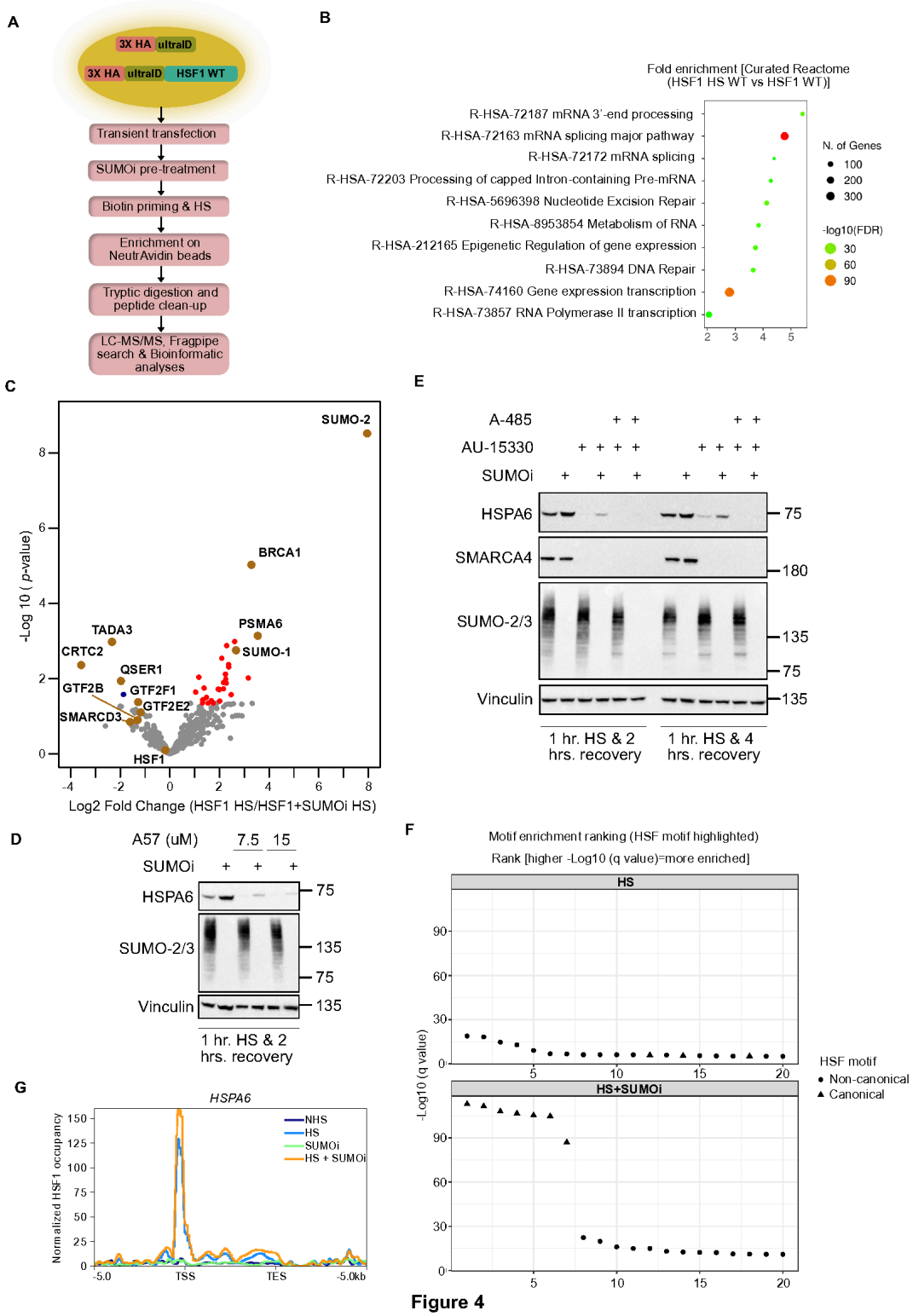

Figure 4

Figure 4

SUMOylation controls the association of HSF1 with transcriptional co-regulators. **(A)**Experimental workflow to identify the proximity proteome of HSF1 WT under control (NHS) and HS in presence and absence of SUMOi (TAK-981; 200 nM). **(B)**HSF1 proximity proteome was filtered first for the candidates which are significantly enriched (Log2 fold change>0.585; -Log10 *p* value>1.34) in any of the Biotin-primed and 3XHA-ultraID-HSF1 transfected conditions over the both no Biotin control (3XHA-ultraID-

HSF1 transfected without Biotin priming) and empty vector control (3XHA-ultraIID transfected with Biotin priming). Subsequently, proteins which are significantly increased (Log2 fold change>0.585; -Log10 *p* value>1.34) in the proximity proteome of HSF1 WT under HS over that of HSF1 WT under NHS were subjected to enrichment analysis based on the Curated Reactome annotations. **(C)** Volcano plot showing the relative fold change (Log2 scale) of proteins in the Biotin-primed and 3XHA-ultraID-HSF1 transfected HS (HS+DMSO) group over the Biotin-primed and 3XHA-ultraID-HSF1 transfected HS+SUMOi group (data is obtained from the proteomics experiment described in A). *P* values for the fold change (represented in the -Log10 scale in the y-axis) were calculated by Paired Student's t test (n=3). Significantly enriched (Log2 fold change>0.585; -Log10 *p* value>1.34) and depleted proteins (Log2 fold change<0.585; -Log10 *p* value>1.34) were coloured red and blue, respectively. Relevant proteins are highlighted and labelled. **(D)** HeLa cells were treated with Artepillin C analog A57 (7.5 and 15μM for 12 h)/DMSO) and were further co-treated with DMSO/SUMOi (TAK-981; 200 nM) for an additional hour before given HS (1 h) followed by recovery (2 h). Whole cell lysates were finally run on SDS-PAGE and immunoblotted to assess the protein levels HSPA6, SUMO-2/3, and Vinculin. **(E)** HeLa cells were treated with A-485 (2.5 μM for 12 h)/DMSO along with AU-15330 (1 μM for 2 h)/DMSO and were further primed with DMSO/SUMOi (TAK-981; 200 nM) for an additional hour. Subsequently, cells were given HS (1 h) followed by recovery (2 and 4 h). Whole cell lysates were finally run on SDS-PAGE and immunoblotted to assess the protein levels HSPA6, SUMO-2/3, SMARCA4, and Vinculin. **(F)** Motif enrichment analysis was performed on CUT&RUN-derived HSF1 peak regions using the MEME Suite. The top 20 enriched motifs were identified based on statistical significance. A rank plot is shown with motifs ordered by significance, displaying the -Log10(q-value) on the y-axis and motif rank on the x-axis (from lowest q-value to higher q-value). Enrichment statistics were derived from SEA output. Motifs classified as "Canonical" correspond to HSF binding motifs, whereas "Non-canonical" denotes non-HSF motifs. **(G)** CUT&RUN was performed for HSF1 under four conditions (NHS, HS, NHS+SUMOi, and HS+SUMOi) and average HSF1 CUT&RUN signal (normalized occupancy, arbitrary units) is shown for *HSPA6*. Signal is plotted across gene bodies scaled from 5 kb upstream of the transcription start site (TSS) to 5 kb downstream of the transcription end site (TES). Profiles represent average signal across biological replicates.

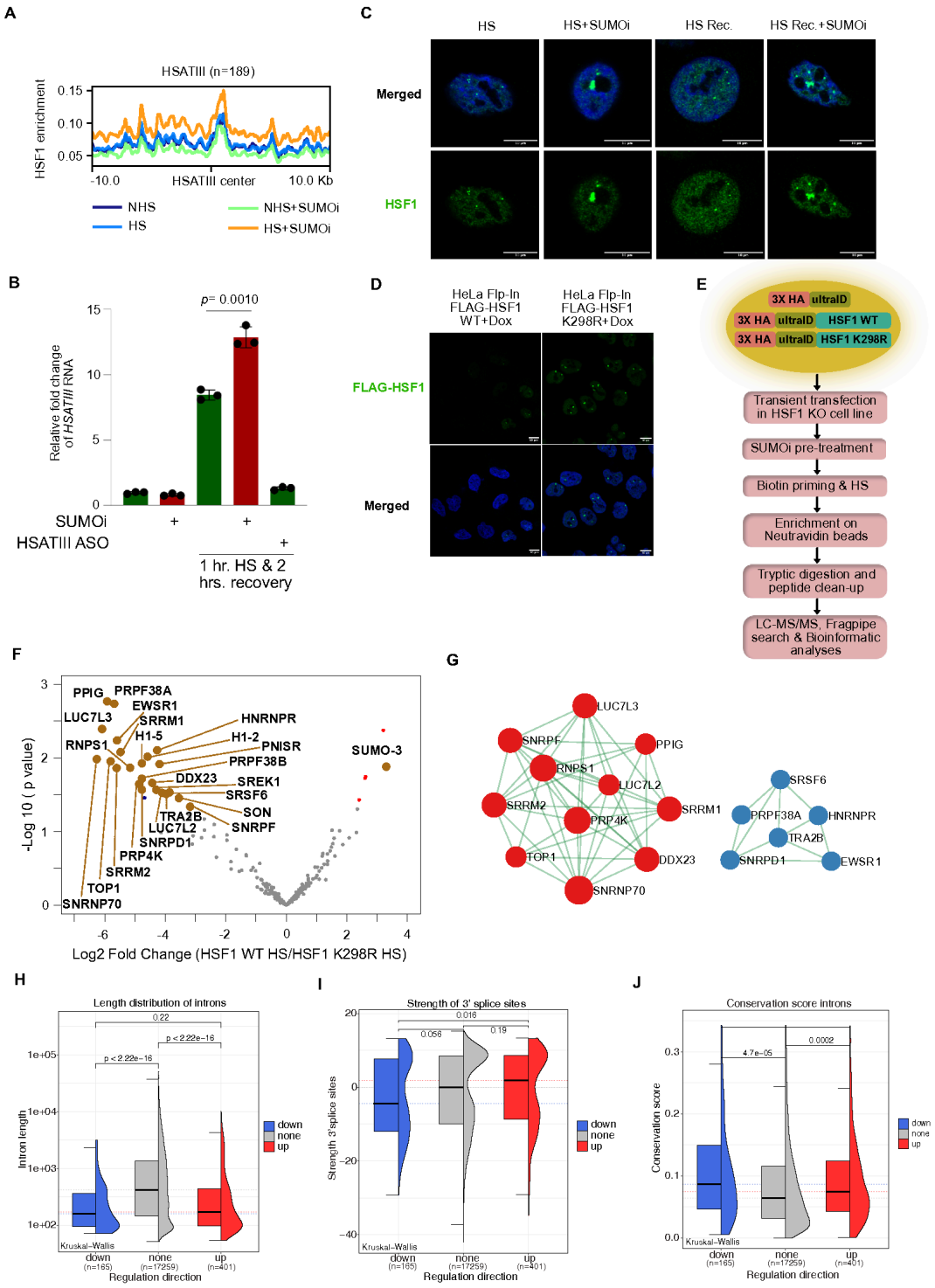

Figure 5

Figure 5

SUMO signaling affects the dynamics of nSBs rewiring mRNA processing. (A) HSF1 CUT&RUN signal was analyzed across n=189 HSATIII loci using a reference-point approach. HSATIII regions were defined based on annotated satellite repeats and merged into non-overlapping intervals. For each interval, the center was calculated as the midpoint between start and end coordinates, and HSF1 signal (±10 kb) was quantified relative to this center. Average profiles of normalized HSF1 occupancy across all HSATIII

regions for four conditions (NHS, HS, SUMOi, HS+SUMOi), with biological replicates combined per condition are shown. **(B)** Control (NHS) and HS-recovered (1 h HS; 2 h recovery) HeLa cells were treated as indicated. Relative fold change of *HSATIII* RNA was quantified by qPCR (normalized against *GAPDH* mRNA) in different treatment groups over the NHS control (NHS+DMSO). Results were shown as mean±standard deviation; *p* value was calculated based on two-sided Student's t-tests (n=3). **(C)** Representative confocal images of the HSF1 positive nSBs in heat-shocked and HS-recovered HeLa cells in the presence of SUMOi (200 nM)/DMSO. Scale bar 10 μm. **(D)** Representative confocal images of the HSF1 positive nSBs in heat-shocked HeLa Flp-In FLAG-HSF1 WT (siHSF1-resistant) and FLAG-HSF1^{K298R} (siHSF1-resistant) cells after 16 hours of Doxycycline (1 μg/ml) priming. Scale bar 10 μm. **(E)** Experimental workflow to identify the proximity proteome of HSF1 WT and HSF1^{K298R} under HS in presence and absence of SUMOi (TAK-981; 200 nM; added only with HSF1^{K298R} transfection). **(F)** Volcano plot showing the relative fold change (Log2 scale) of proteins under HS in the Biotin-primed, 3XHA-ultraID-HSF1 WT transfected group over the Biotin-primed, 3XHA-ultraID-HSF1^{K298R} transfected group (data are obtained from the proteomics experiment described in E). *P* values for the fold change (represented in the -Log10 scale in the y-axis) were calculated by Paired Student's t test (n=3). Significantly enriched (Log2 fold change>0.585; -Log10 *p* value>1.34) and depleted proteins (Log2 fold change<0.585; -Log10 *p* value>1.34) were coloured red and blue, respectively. Relevant proteins are highlighted and labelled. **(G)** Cytoscape network of selected proteins highlighted and designated in Figure F. **(H, I, J)** Comparison of the length distribution (**H**), the strength of 3'splice sites (**I**) and the conservation scores (**J**) in introns that were up-regulated (401), down-regulated (165) or not regulated (17259) during heat stress recovery and SUMO inhibition.

Supplementary Files

This is a list of supplementary files associated with this preprint. Click to download.

- TableS7.xlsx
- TableS6.xlsx
- TableS8.xlsx
- TableS5.xlsx
- TableS1.xlsx
- TableS4.xlsx
- TableS3.xlsx
- TableS2.xlsx
- SupplementaryFigures15Legends.pdf